THESIS FOR THE DEGREE OF LICENTIATE OF ENGINEERING

Micro-grinding of titanium

Mohammadali Kadivar

Department of Industrial and Materials Science

CHALMERS UNIVERSITY OF TECHNOLOGY

Gothenburg, Sweden 2018

Micro-grinding of titanium
Mohammadali Kadivar

Technical report no IMS-2018-17

Department of Industrial and Materials Science
Chalmers University of Technology
SE-412 96 Gothenburg
Sweden
Telephone + 46 (0)31-772 1000

Printed by Chalmers Reproservice
Gothenburg, Sweden 2018

To my beloved mother Tooran and nieces Sara and Saina

Micro-grinding of titanium

Mohammadali Kadivar

Department of Industrial and Materials Science
Chalmers University of Technology

Abstract

Titanium and its alloys are difficult-to-cut materials, commonly used in several application fields, such as: medicine, aerospace, automotive and turbine manufacturing due to their biocompatibility, corrosion resistance, excellent mechanical and thermal properties, and light weight. However, its machining is associated with several difficulties, such as high tool wear, low surface quality, high cutting forces and high costs. To overcome these problems, using a proper and efficient manufacturing process seems essential. Micro-grinding provides a competitive edge in the fabrication of small-sized features and parts with superior surface quality compared with other processes. The quality aspects such as surface integrity of the parts produced by micro-grinding is influenced by various factors related to the induced mechanical and thermal loads during the process. Therefore, the machining parameters must be carefully chosen and controlled. Hence, developing an advanced, highly effective and efficient method, which can produce high quality micro-parts without inducing sub-surface damage, seems essential.

In this study, experimental and analytical investigations on 2D micro-grinding of titanium are presented. The run-out of micro-tools can be affected by the relatively high forces induces by mechanical dressing, meaning that the dressing and tool-conditioning possibilities are limited. Therefore, a proper set of dressing parameters is obtained for dressing of micro-grinding tools. An analytical model, which considers grits interaction, heat transfer and actual micro-grinding tool topography is developed which is able to predict the surface roughness and cutting forces for a given set of dressing and grinding parameters. It is shown that the topography of the tool varies with changing the dressing parameter which affects the grinding forces and surface roughness. In the analytical model the actual topography of the tool is considered in the simulation for the first time. Additionally, the model is able to determine grinding parameters that generate minimum surface roughness with minimizing the grinding forces. To determine the correct chip thickness with the maximum material removal rate, an appropriate grinding tool and optimum process parameters to generate highly accurate contours in a micron scale will be further analyzed.

Using the analytical model, the effects of process parameters and tool surface topography are mapped to the process outputs, i.e. surface roughness and grinding forces. The results show that the analytical model enables the prediction of micro-grinding forces with a total error of 13.5% and surface roughness with the total error of 16%. The simulation results match with the experimental results to a greater degree in the low cutting speed range, rather than at higher cutting speeds. The results also indicate that the dressing parameters, such as the dressing overlap ratio and the speed ratio are influential factors, affecting surface roughness and grinding forces. Using higher values of dressing overlap ratio (U_d up to 1830) reduced the surface roughness, however, leads to approximately 70% higher cutting forces. The observed 40% reduction in the grinding forces is achieved by increasing the cutting speed from 6 to 14 m/s, but this increases the surface roughness. Higher values of the dressing overlap ratio reduce the chip cold-welding on the abrasive grains and causes less loading of the tool in form of chip nests. Welded clogging of the grinding pin at lower U_d values deteriorates the surface quality resulting in increased surface roughness. Using the up-dressing method leads to lower chip loading over the surface of the grinding tool, which improves the ground surface. Moreover, the down-dressing of micro-grinding pins results in higher value of surface roughness and lower grinding forces compared with up-dressing.

Keywords: Micro machining, dressing, modelling, grinding, tool topography.

Preface

This licentiate thesis is based on the work performed at the Institute for Precision Machining (KSF) at Hochschule Furtwangen University (Germany) between April 2016 and October 2018. The research has been carried out under the main supervision of Professor Dr.-Ing. Bahman Azarhoushang from KSF and co-supervision by Professor Peter Krajnik and Professor Uta Klement, both at the Department of Industrial and Materials Science at Chalmers University of Technology.

This Thesis consists of an introductory part followed by the appended technical papers:

Paper I: **The effect of dressing parameters on micro-grinding of titanium alloy**

Mohammadali Kadivar, Bahman Azarhoushang, Sergey Shamray, Peter Krajnik

Precision Engineering 51 (2018): 176-185.

§ Paper 1: The author participated in the planning of experiments with the co-authors, performed the experiments, all characterization work, measurments, and data analysis, as wel as writting the paper in cooperation with the co-authors.

Paper II: **Modelling of the micro-grinding process considering the grinding tool topography**

Mohammadali Kadivar, Ali Zahedi, Bahman Azarhoushang, Peter Krajnik

International Journal of Abrasive Technology 8.2 (2017): 157-170.

§ Paper 2: The author planed the design of experiments with the co-authors, performed the experiments, and participated in the simulation study with co-authors, and validated the results. The author also wrote the paper in cooperation with the co-authors.

Paper III: **The effect of dressing parameters on the chip loading and ground surface quality by using grinding pins and grinding wheels with very fine grits**

Mohammadali Kadivar, Heike Kitzig-Frank, Bahman Azarhoushang

Fourth European Seminar on Precision Optics Manufacturing. Vol. 10326. International Society for Optics and Photonics, 2017.

§ Paper 3: The author disigend the experiments regadring micro-grinding tests with the co-authors, performed the experiments, measurments, and data analysis regadring micro-grinding tests. The author also wrote the paper in cooperation with the co-authors.

Contents

1. Introduction and State-of-the-art

The society demands are forcing the companies to introduce new micro-parts and new manufacturing process. Consequently, new manufacturing-application fields are opened which are becoming more and more interesting for the researchers and industries [1]. There are several methods to manufacture parts in micro-size which are categorized into two groups: (1) non-mechanical and (2) mechanical micro-manufacturing. Non-mechanical micro-manufacturing methods such as lithography, Electro Discharge Machining (EDM), and chemical machining are expensive, the process time is always long and are normally not suitable specially in the case of small-batches [2]. Another problem is the dependency of such processes to the type of the machined material and are in some cases only suitable for some specific materials. For instant, only conductive materials can be machined using EDM. Hence, using mechanical manufacturing methods seem highly important.

Mechanical micro-cutting is one of the key technologies to enable the realization of high accuracy complex micro-products made from a variety of engineering materials including titanium and its alloy, with high accuracy and capability of producing complex micro-parts 3D geometry. Micro-cutting raises a great number of issues, mainly due to the size or scale associated with the process. The size effects can change the whole aspect of the machining process. Since the ratio of size of part/size or the micro-structure to the cutting tool dimension/cutting parameters becomes smaller as the results of size effect. Furthermore, scientific understanding of fundamentals and applications in micro-machining is essential and much needed to address the underlying necessities for predictability, producibility, repeatability and productivity of manufacturing at micro-scales [1].

In principle the micro-cutting processes are kinematically similar to conventional cutting processes. However, they are fundamentally different in several aspects which are listed below [1]:

1- Uncut chip thickness and underlying cutting mechanics: The uncut chip thickness in the micro-cutting processes differ from that in macro-cutting process and is much smaller. It is impossible to scale down the macro-cutting processes to micro-cutting since in micro-cutting processes the uncut chip thickness becomes comparable to the grain size of workpiece materials. In this case some issues which are not important in macro-cutting become critically important in micro-cutting such as cutting-edge radius effect, tool-workpiece contact at the flank face, minimum chip thickness and micro-structure effect. The aforementioned points are known as size effect. Moreover, machining dynamics is also totally different because of the size of the tool and machine tool.
2- Dimensions and accuracy of micro-parts or features: micro-cutting process is being used for producing the part with small size or the parts including micro-features and micro-structures which may have the range of 1–1000 μm with relative accuracy in the order of 10^{-3}–10^{-5} and surface roughness (Ra) less than 100 nm.
3- Cutting tool geometry: in micro-cutting the size and the shape of the micro-tools is limited to the size and accuracy of micro-features. The tool diameters are typically in a range from 25 μm up to 2000 μm. Thus, the micro-geometry is becoming very important.
4- Application area: micro-cutting has a broad application in areas requiring micro-components and is capable to machine wide range of engineering materials including titanium, metals, polymers, technical ceramics and composites.

But choosing a proper micro-machining process is an important issue. Among the micro-mechanical machining processes, grinding has gained a lot of attention as the final finishing process. Micro-grinding is an effective process to achieve dimensionally high accurate parts with superior finished surface.

1.1. Titanium

Difficult-to-cut materials such as titanium and its alloys are commonly used several application fields. Titanium has superior properties such as great strength property, high strength-to-weight ratio, corrosion resistance, biocompatibility, good mechanical properties, and lightweight [3]. The aforementioned advantages make this material suitable for the fabrication of parts and devices for biomedical applications such as implantable drug-delivery systems and micro-surgery tools [4]. The best example are biomedical implants (Fig. 1). In this case the biological performances of titanium implants are highly dependent on their surface topography for example knee joints [5]. It also has long been used for macro-scale biomedical devices like orthopedic and micro-needles [6]. Since the demand for these micro-parts is increasing, more and more companies and research groups are getting involved with the micro-machining of this material. However, machinability of these materials is facing several challenges. For example, high tool wear associated with the reactivity of titanium with tool materials, and its low thermal conductivity [7]. Burr formation also can be counted as one of the limitations [8].

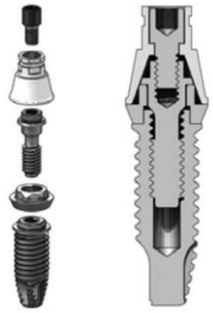

Fig. 1. Dental implant components. (Reprinted by permission from Springer: Springer Nature, the journal of the Minerals, Metals & Materials Society, [9], Titanium in medicine: Material science, surface science, engineering, Brunette DM, Tengvall P, Textor M, Thomsen, Copyright (2013)).

As far as biomedical applications are concerned, a huge number of topographical features in the nano-, micro- and meso-scale is needed, mainly for implants in bone structures. For load-bearing implants, parts in the range of over 100 μm are needed and are essential for the mechanical interlocking of bone tissue to provide better osteo-integration, like the intimate contact between the bone tissue and the surface of titanium implants [10]. The other examples are including artificial hip joints, artificial knee joints, and bone plates, screws for fracture fixation, cardiac valve prostheses, pacemakers, artificial hearts, crowns, bridges, overdentures, and dental implant prosthesis components (screw and abutment) [9]. Another dentistry example is a temporary orthodontic mini-implant used generally to secure anchorage in contemporary orthodontic treatments (Fig. 2). This implant has a small diameter (1.2 mm to 2.0 mm) and the orthodontic load can deform the mini-implant [9]. One of the most important criteria for such parts is the surface roughness which affects many implant-cell interaction parameters and must be carefully controlled, especially the parts that are in direct contact with the bloodstream.

Fig. 2. An example of an orthodontic mini-implant for anchorage application. (Reprinted by permission from Springer: Springer Nature, the journal of the Minerals, Metals & Materials Society, [9], Titanium in medicine: Material science, surface science, engineering, Brunette DM, Tengvall P, Textor M, Thomsen, Copyright (2013)).

Titanium and its alloy can be also used as a good replacement in Micro-Electro Mechanical Systems (MEMS) and micro-needles [6,11–13]. Recent process developments have permitted to use titanium to produce and fabricate of MEMS (Fig. 3). The material has several advantages that make it more attractive than single-crystal silicon in the field of MEMS [11,13,14]. First, as a metal it has inherently higher fracture toughness than silicon and other semiconductor materials [15,16]. Second, it has a greater biocompatibility, makes it suitable for many applications in vivo.

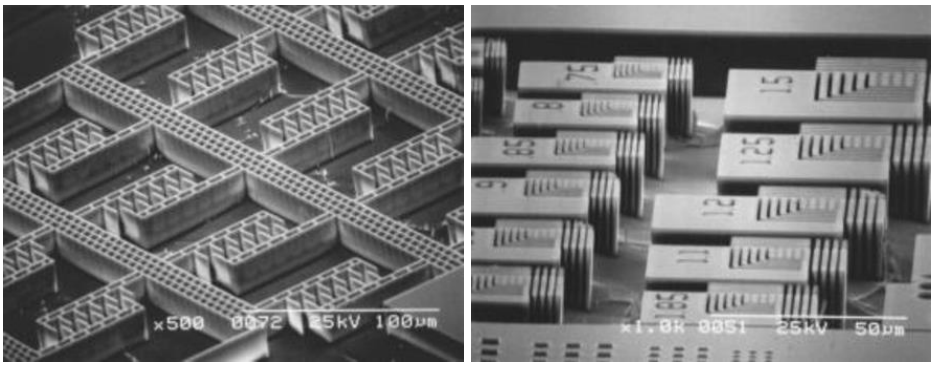

Fig. 3. Left: Scanning electron micrograph of a titanium-based MEMS comb drive structure, right: Scanning electron micrograph illustrating sub-micrometer minimum feature size capability. (Republished with permission of Journal of the Electrochemical Society, from Inductively Coupled Plasma Etching of Bulk Titanium for MEMS Applications, Parker ER, Thibeault BJ, Aimi MF, Rao MP, MacDonald NC, 152, 10, 2005).

Titanium is also used as a common material in aerospace industries [7]. Furthermore, this material has a high temperature retention strength, good creep- and oxidation-resistance properties. These devices are continuously growing with emerging trend in miniaturization of turbines (Fig. 4), valves, seal supports, cases of fire resistant micro-systems, power generation, oil and gas extraction, titanium-based micro-aerial vehicle wings, and other major industries [11,17–21].

1.2. Micro-cutting

The possibility for manufacturing the miniaturized parts is clearly beyond the capability of current machine tools. Producing the micro-parts requires the use of a specific, and carefully controlled machining procedure to achieve, easily fabricated, less expensive, high performance and high-quality micro-parts with complex geometry and high dimensional accuracy. The

emergence of miniature and micro-products in the last one or two decades is increasingly demanding the production of components and products with dimensions in the range of a few tens of nanometers to some few millimeters (Fig. 5) [22].

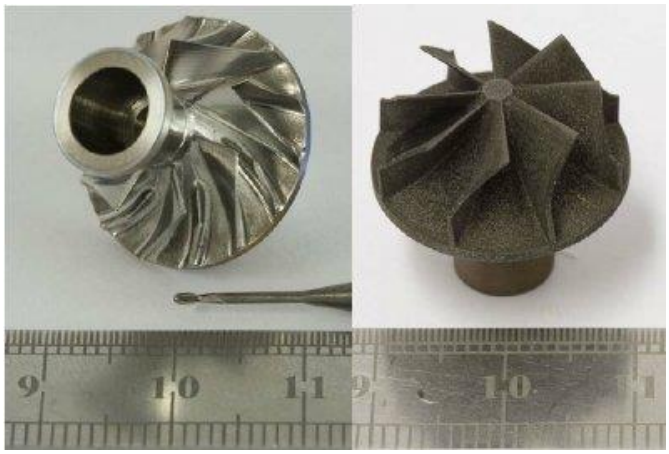

Fig. 4. Micro-turbine impellers from titanium © 2015 IEEE. (Reprinted, with permission, from Robinson AE, Funke H, Hendrick P, Recker E, Peirs J. Development of a hydrogen fueled 1 kW ultra-micro gas turbine with special respect to designing, testing and mapping of the µ-scale combustor, 2008 IEEE International Conference on Sustainable Energy Technologies, Nov/2008).

Research has been carried out in micro-cutting mechanisms for decades and experimental studies still dominate the micro-cutting research. Some analytical and numerical models for micro-cutting have been developed based on conventional cutting models and some size effects have been incorporated into these models. High-accuracy mechanical miniature components with dimensions ranging from hundred microns to a few millimeters or features ranging from a few millimeters to a few hundred microns are increasingly in demand for various industries, such as aerospace, precision engineering, medical engineering, biotechnology, electronics, communications and optics. Special applications include fuel cells, micro-fluidics, moulds for micro-optics/lenses and fiber optic elements, micro-nozzles, to name a few. Many applications require very tight tolerances and both functional and structural requirements demand the use of various engineering materials, including stainless steel, titanium, brass, aluminum, plastics, ceramics and composites [1,11,22,23]. The desired surface finish in micro or nano-range is another issue in the micro-manufacturing that should be strictly considered and monitored.

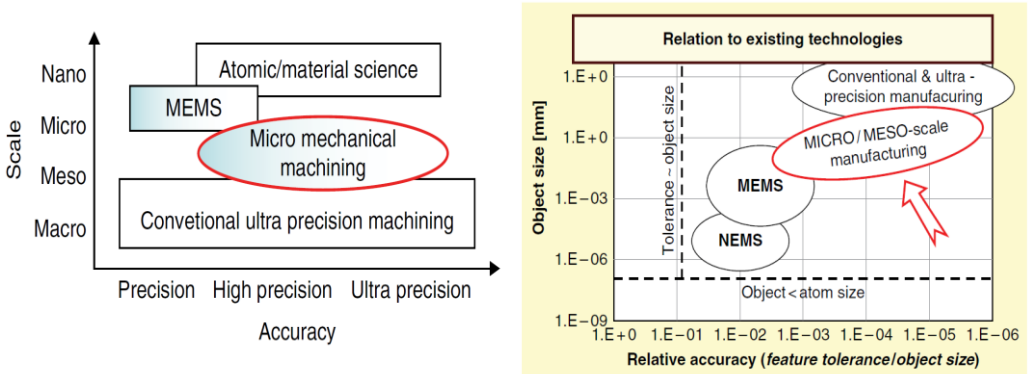

Fig. 5. Left: dimensional size for the micro-mechanical machining (Reprinted with permission from Wiley, Dehong Huo and Kai Cheng, Micro-Cutting: Fundamentals and Applications, John Wiley and Sons) [1]; right: micro-manufacturing size/precision domains (Reprinted from International Journal of Machine Tools and Manufacture, 46/3-4, Chae J, Park SS, Freiheit T, Investigation of micro-cutting operations, 313–332, Copyright (2006), with permission from Elsevier).

It has long been known that traditional micro-manufacturing processes, such as chemical etching and lithography, cannot match future demand of the industry for micro-parts, since these micro-manufacturing methods are generally planar processes and applicable just for semiconductor materials. The relative accuracies of micro-manufacturing processes are of the order of 10^{-1} to 10^{-2}, whereas the needs of many mechanical miniaturized parts need relatively more accuracies such as in the order of 10^{-3} to 10^{-5} [22] . On the other hand, many applications of the micro-parts also need high surface quality such as the surface roughness of the machined surface. Micro-cutting can overcome these problems and achieve aforementioned requirements of the machining 3D high accurate micro-parts in a wide range of engineering materials. Fig. 5 (left) compares dimensional size and accuracy with other manufacturing methods.

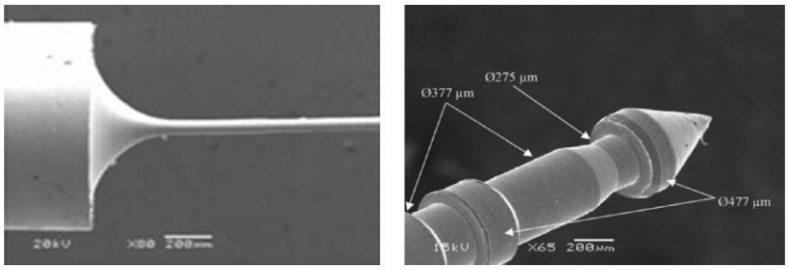

Fig. 6. Simple and compound shaped micro-pin by micro-turning (Reprinted with permission from Wiley, Dehong Huo and Kai Cheng, Micro-Cutting: Fundamentals and Applications, John Wiley and Sons).

Fig. 5 (right) illustrates micro-manufacturing size/precision domains. Micro-cutting is normally used to produce part or features with sizes ranging from tens or hundreds of microns (Fig. 6). Although micro-machining may not be capable of producing the smallest feature size as would be the case using MEMS and NEMS (Nano Electric Mechanical Systems) processes, it is a critical technology in bridging the gap between macro and nano-domain [23]

1.3. Micro-grinding

Micro-grinding is an effective process to achieve high dimensionally accurate parts in machining process with superior surface finish. Due to its capability to generate superior surface integrity, micro-grinding is normally used as the final production procedure. Unlike other micro-cutting processes (turning and milling) where ductile or less hard materials are usually machined, micro-grinding is capable to machine also brittle and hard to cut materials. In the case of high accuracy, when the micro-features do not require micro-grinding tools, the relatively large grinding wheels can be used. However, the size and geometry of micro-grinding tools determine the limit of the size and geometry of micro-parts and micro-features [24]. Fig. 7 shows two different micro-grinding tools with very small sizes.

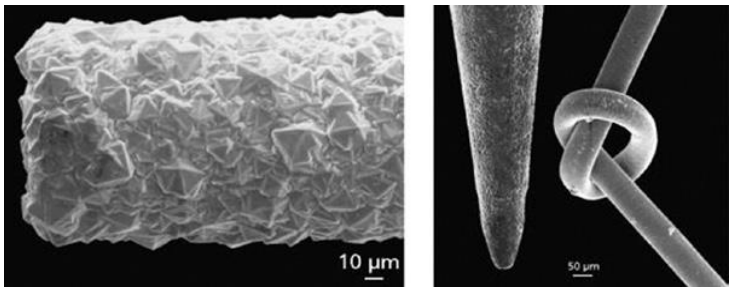

Fig. 7. Micro-CVD diamond-coated grinding tools (Reprinted from International Journal of Machine Tools and Manufacture, 50/4, Jan Gäbler, Sven Pleger, Precision and micro CVD diamond-coated grinding tools, 420–424, Copyright (2010), with permission from Elsevier).

The micro-grinding process offers certain advantages over other mechanical micro-machining technologies and has been researched in several studies. Producing the micro-feature and micro-parts with the highest quality is a mean goal of micro-grinding which in this case it outperforms other micro-cutting processes. Cao et al [25] showed that 3D micro-structures with high surface quality can be effectively machined (Fig. 8) with combination of Electrochemical Discharge Machining (ECDM) and Polycrystalline Diamond (PCD) grinding and the machining time can be reduced up to 30 percent with higher surface quality.

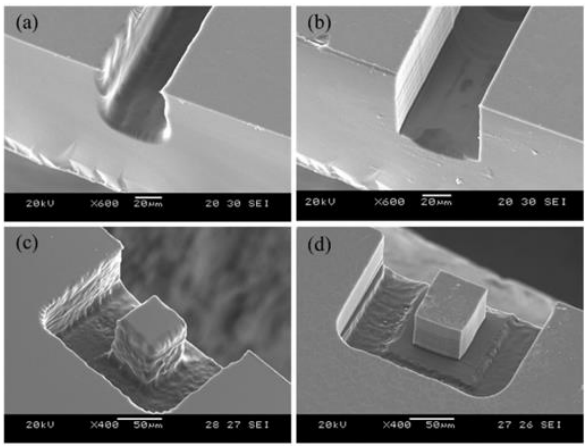

Fig. 8. Micro-structures machined by (a,c) ECDM and (b,d) then ground by a PCD tool. (Reprinted from International Journal of Precision Engineering and Manufacturing, 14/1, Xuan Doan Cao, Bo Hyun Kim, Chong Nam Chu, Hybrid micromachining of glass using ECDM and micro grinding, 5–10, Copyright (2013), with permission from Elsevier).

The effect of micro-grinding parameters on surface quality and subsurface recrystallization of nickel based single-crystal super-alloys was studied by Zhou et al. [26]. They showed that micro-grinding process with lower cutting speeds, higher feed rates and depth of cuts, led to a higher level of tool wear. However, the surface quality became gradually worse. Moreover, the lubrication could improve the tool life and surface quality. They also observed that the wear of abrasives was the main wear form of micro-grinding tool in the early stage.

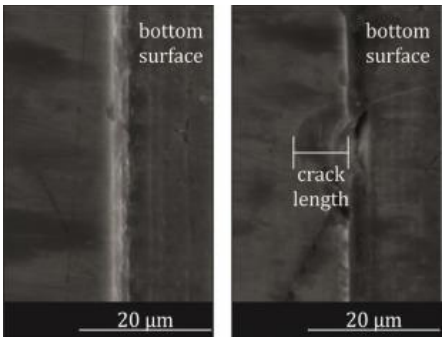

Fig. 9. Edge crack length for C100–C145 and grain size of 1 μm (left) and C100–C145 and grain size of 2 μm (right). (Reprinted from CIRP Annals - Manufacturing Technology, 64/1, Aurich JC, Carrella M, Walk M, Micro grinding with ultra-small micro pencil grinding tools using an integrated machine tool, 325–328, Copyright (2015), with permission from Elsevier).

Feng et al. [27] monitored tool wear during micro-grinding of ceramic and showed that without knowing the machining characteristics, the tool wear monitoring is possible. They also presented a simulation model to predict the generated surface by the micro-grinding process [28]. Aurich et al. [2] studied the influence of micro-grinding pins' specification on the material removal mechanism of silicon. They showed that, the smaller the grain sizes and the smaller

the grain concentrations, the better the structure quality and the higher the tool wear. Decreasing the feed rate and increasing the cutting speed improved the surface quality. They also showed that using smaller tool diameters caused large edge cracks at the edge of the machined area (Fig. 9).

Butler-Smith et al. [29] presented a new laser-generated diamond micro-grinding tool (Fig. 10) for titanium micro-machining. The new tool was conceited of highly uniform cutting elements with an optimized layout. This ensures an even distribution of load during the micro-grinding process. Moreover, the material removal is ideally shared, and an efficient chip flow occurs during the process. Therefore, the new tool outperformed conventional electroplated diamond micro-grinding tools for precise applications. A superior finished surface (three times better than the one induced by a conventional tool) could be achieved with the newly developed tool and better durability was accomplished.

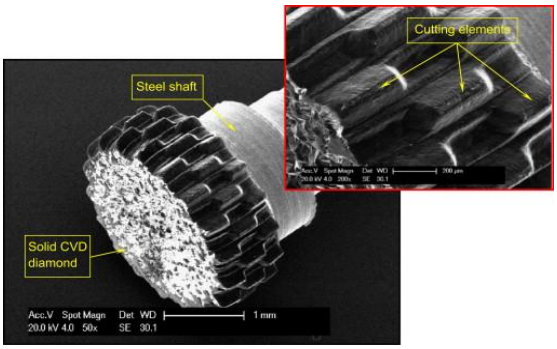

Fig. 10. Unused laser ablated solid diamond micro-grinding tool (Reprinted from International Journal of Machine Tools and Manufacture, 59/August, Butler-Smith PW, Axinte DA, Daine M, Solid diamond micro-grinding tools: From innovative design and fabrication to preliminary performance evaluation in Ti–6Al–4V, 55–64, Copyright (2012), with permission from Elsevier).

Feasibility of Minimum Quantity Lubrication (MQL) in micro-grinding has been investigated by Lee et al [30]. They proved that using nanofluid MQL can reduce the grinding forces and improve surface roughness significantly. In the case of grinding forces, the nano-diamond particles used in MQL as well as higher volumetric concentration of the diamond particles and smaller size are more effective than nano-Al_2O_3 particles. However, the Nano-Al_2O_3 particles performed more effective than nano-diamond particles in the case of surface roughness. This cooling-lubrication method can also improve the tribological properties [31].

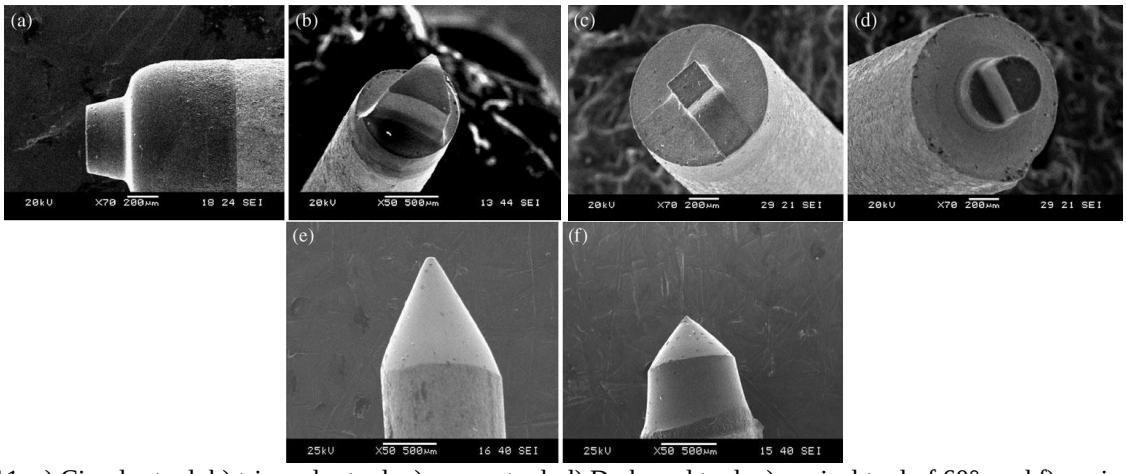

Fig. 11. a) Circular tool, b) triangular tool, c) square tool, d) D-shaped tool, e) conical tool of 60°, and f) conical tool of 90°. (Reprinted by permission from Springer: Springer Nature, The International Journal of Advanced Manufacturing Technology, [32], Fabrication of different geometry cutting tools and their effect on the vertical micro-grinding of BK7 glass, Asma Perveen, Wong Yoke San, Mustafizur Rahman, Copyright (2013)).

In contrast with macro-grinding, the micro-grinding tool can have irregular shapes. Perveen et al. [32] investigated the performance of the PCD tools with different geometries produced by EDM process for glass micro-grinding (see Fig. 11). The results indicated that the lowest grinding force in tangential and normal directions were induced using D-shaped tool, whereas triangular tool experienced lower force along z-axes (parallel to the tool axis), and the highest grinding force was induced by the circular tool. The surface roughens was much finer when the circular tool was used. The tool wear was higher in the case of square and triangular tools compared to circular and D-shaped tools. Overall, the D-shaped tool performed better compared to the other geometries.

Morgan et al. [33] used a PCD D-shaped tool to produce the micro-holes via grinding in tungsten carbide. The results showed that the straightness, waviness, and roughness of the drilled holes can be improved using the new formed tool. In another study they used another shape of the tool (see Fig. 12) to grind glasses [34]. Using higher depth of cut caused brittle fractures around the edges of the grooves. When the depth of cut was lower than the critical chip thickness brittle fractures were not observed, and the ductile mode was obvious. Moreover, the surface roughness of around 0.3 nm was achievable using the new tool.

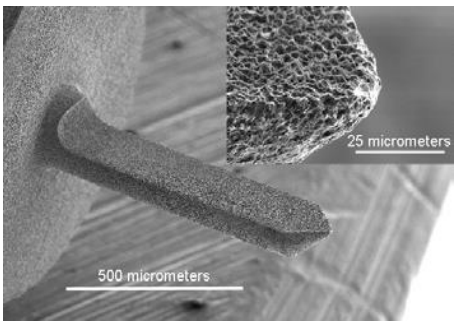

Fig. 12. SEM image of a conical tipped PCD tool. (Republished with permission of IOPscience, from Micro machining glass with polycrystalline diamond tools shaped by micro electro discharge machining, Morgan CJ, Vallance RR, Marsh ER, 14, 12 and 2004).

Another important factor in micro-grinding is the specific grinding energy defined as the energy expended per unit volume of material removed. Morgan et al. [35] used the metrology data to examine the surface quality of the ground groove in tungsten carbide. They measured the grinding forces in the normal direction to the feed speed to calculate the specific grinding energy. The specific grinding energy remained constant after tool entrance and did not changed while increasing the contact length. They found that the tool round-out has a great influence in the micro-grinding forces measurements at a frequency equal to the spindle speed.

In longer machining cycles the effect of grinding temperature on the quality and performance of the parts becomes more important and critical to investigate. Yadong et al. [36] studied the temperature distribution on the ground surface in micro-grinding of H26 steel by the means of experiment and finite element simulation. Since the grinding forces were relatively small compared to the macro-grinding process, the grinding temperature was not high. They measured the highest temperature at the depth of cut of 0.022 mm which was just about 53ºC.

1.4. Modeling

Modelling of the micro-grinding process, especially micro-grinding forces and surface roughness plays an important role in characterizing the micro-cutting mechanisms. In conventional grinding process there exist a lot of modelling methods which can be categorized

into three groups according to: analytical methods, experimental methods and numerical methods [37–39]. Analytical modelling of the micro-cutting process is still at its early stage. There are only a few effective models to predict the micro-grinding process. There are two approaches to analytically model the grinding forces [1]. The first approach calculates cutting forces using the instantaneous uncut chip cross section, and the second one is based on a slip line field model which calculates cutting forces using the shear plane area [1]. Most of the models are adapted from the two conventional approaches, but taking one or more size effects into consideration. The size effects which have been modelled to predict micro-cutting forces include ratio of feed rate to tool radius; cutter edge radius [40]; minimum chip thickness [41]; and micro-structure effect.

The chip thickness in micro-grinding is relatively small compared to macro-grinding. Thus, mechanical and thermal interactions between a single grit and the material which is removed are linked to the size effect phenomena. Here the generated surface is not only related to the process parameters and micro-grinding wheel properties, but also the microstructure of removed material, accordingly the crystallographic effect should be also considered in micro-machining. On the other hand, the diameter of the tool in micro-machining is much smaller than those in macro-machining. Thus, the ploughing and friction forces which are normally neglected in macro-machining become more significant. Moreover, in micro-grinding the grinding tool deformation and deflection become more critical. These phenomena are not only related to the size of the tool, but also to the physical mechanisms of the material removal process (Fig. 13) [42], affecting both cutting forces and surface roughness.

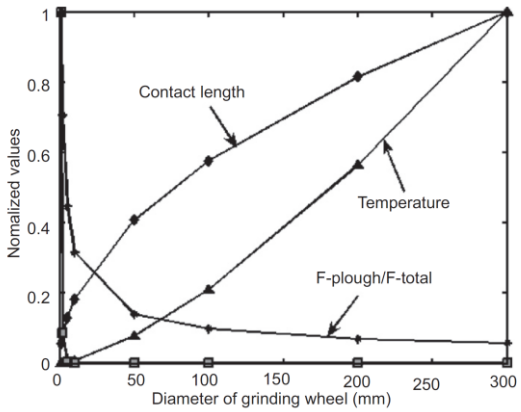

Fig. 13. Variation trend of main parameters according to varying wheel dimensions (Reprinted from International Journal of Machine Tools and Manufacture, 48/15, Hyung Wook Park,Steven Y. Liang, Force modeling of micro-grinding incorporating crystallographic effects, 1658–1667, Copyright (2008), with permission from Elsevier).

The ground surface roughness resulting from micro-grinding has a significant influence on the performance of micro-parts. It is believed that surface integrity, dynamics performances and electrostatic characteristics of micro-components strongly depend on the achieved micro-machined surfaces parameters in terms of surface integrity (including surface roughness). Therefore, the quantitative characterization of the micro-machined surfaces and corresponding optimization of machining parameters is much desired. The size effect has a significant influence on the generated surface roughness in micro-machining. The surface roughness can be also described as a function of the equivalent chip thickness. This can be considered as a subclass of empirical models due to the empirical constants that need to be adjusted [42].

In micro-machining processes there is an optimal value for the feed rate which produces the smallest surface roughness and is related to the minimum chip thickness. A typical surface is characterized by finishing cutting paths and plowed material to the sideway of grooves.

However, many other marks can be found such as cracks produced by thermal impact, back transferred material, and craters produced by grain fracture [43]. Other factors that characterize a ground surface are the traverse and longitudinal waviness produced by the random nature of the grinding process and by machining vibration. When considering all these factors, a complete prediction of the surface topography is a complicated problem.

Analytical models for surface roughness are based on the micro-structure of the micro-grinding tool in both one and two dimensions [1]. The tool topography is described using simplification factors such as constant distance between cutting edges and uniform height of the cutting edges. Similar assumptions are used to describe the surface roughness based on chip-thickness models. The number of cutting edges over the surface of the micro-tool are limited and the wheel topography has a significant effect on the generated surface roughness [1]. Moreover, the parameters such as grit protrusion heights, inter-grit spacing, and grit locations play a very crucial role in the modeling as well. The first step in these modeling approaches is the prediction of micro-tool topography. Like in macro-grinding the abrasive grains are stochastically distributed over the surface of the grinding tool in micro-grinding, and it is difficult to model the exact topography of the micro-grinding tool. Anandita et al. [44] studied the kinematic effects of tool topography and process parameters on the generated surface in micro-grinding process. They generated the micro-grinding tool considering all the realistic randomness from an electroplated micro-grinding tool. They also proposed an algorithm to minimize the clustering of grits in order to guarantee an appropriate homogeneous grit distribution over the micro-grinding tool surface. Kunz and Mayor [45] used the machine vision analysis to measure the static grit density of the abrasive grains in micro-grinding and provided probability distributions for the static grit density.

The micro-grinding temperature is another important factor which has been model by Gorodkova et al [46]. Their proposed thermo-physical model allowed to calculate the cutting zone temperature and the temperature distribution over the ground surface as a function of process parameters such as the cutting speed, the feed rate, the cutting depth, and the material properties.

2. Research objectives

This work will present experimental and modeling studies on micro-grinding of titanium. Up to now, the understanding of the effects of micro-grinding parameters on workpiece surface quality is still vague. Moreover, the research addressing the micro-precise contour production on hard-to-cut materials by micro-grinding is limited. Additionally, the micro-grinding of titanium has not been fully investigated, yet. Dressing and tool conditioning, which directly influence the surface quality and grinding forces, have been neglected by researchers and there is no analytical study or dedicated modeling available considering the effects of dressing parameters on the grinding process outputs.

In this thesis a methodology for predicting the micro-grinding forces and surface roughness has been introduced – based on analytical analysis of the process. For the first time, the effects of the dressing parameters on micro-grinding forces and surface roughness are investigated. The analysis considers the single-grit interaction and micro-grinding tool topography. The results have been validated with experimental tests. In experimental work, diamond grinding tools have been used to generate accurate contours, to achieve the above-mentioned objectives. An appropriate grinding tool to generate and desired surface quality, along with optimal grinding and dressing parameters have been determined. Moreover, a chip-thickness threshold has been proposed for achieving maximum material removal. Mechanical dressing technique using a diamond roller has been used for dressing the grinding tool, and its effect on surface quality and forces has been studied.

The goal of this project is to investigate the effect of grinding and conditioning parameters on the chip formation mechanism, micro-grinding forces, and surface quality, chip loading and present a mathematical and analytical model for the process.

3. Analytical/theoretical work

The number of research papers in the field of micro-grinding process are mainly limited to study of the grindability of various materials, and there is a lack of modelling studies in this field. In this thesis, the single-grain scratch test results for titanium have been adopted from the work of Feng and Cai [47]. Based on these experimental data, a regression model has been extracted for the normal grain force and pile-up characteristics as functions of grain size, cutting speed, and depth of cut. The results for single-grain scratch, i.e., the force values and the chipping mechanism have been further extended to the aggregate action of the cutting grains in the grinding process through the kinematics of the process. The simulated forces and surface roughness have also been validated by the experimental results in micro-grinding of Ti6Al-4V.

3.1. Single-grain scratch

The experimental results for single grain scratch test of the Ti6Al-4V were extracted from Feng and Cai [47] work, where experiments were performed at different cutting speeds and depth of cuts. The results for grinding normal and tangential forces (F_{ng} and F_{tg}), which correspond to different grain cross-section areas (A_g) are shown in Fig. 14. The cross section was measured after single grain test considering the plastic deformation and piled up. The cross-section area of grain and workpiece engagement could be directly related to the depth of cut and the average grain size (assuming that the tip of the abrasive grain has a spherical form).

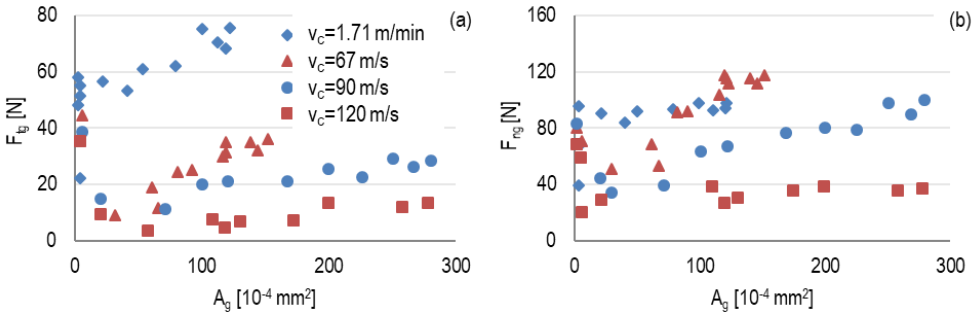

Fig. 14. Single-grit grinding forces: a) normal grinding force, b) tangential grinding force [47]

Higher cutting speeds led to lower forces which constantly increased with the increase of the A_g. Increasing the cutting speed reduces the plowing and sliding in the process. The grinding forces consist of cutting, plowing, and sliding components [48]. The proportional relation between the forces and flat wear area implies a constant average contact pressure $\bar{\rho}$ and friction coefficient μ between the wear flat and work material, where these relationships can be expressed as follows:

$$F_{ng} = \mathrm{kA_g} + \delta\bar{\rho} \quad (1)$$

$$F_{tg} = \emptyset \mathrm{k\ A_g} + \mu\delta\bar{\rho} \quad (2)$$

where, F_{ng} and F_{tg} are normal and tangential forces in single grain test, k is the specific grinding force acting upon a unit grinding section area, $\emptyset$ the coefficient relating to half cone

angle of the grain, δ is the actual area of contact between the wear flats and the workpiece. The ratio of F_{tg}/F_{ng} can be derived from Eqs. 2 and 3 as:

$$\varepsilon = \frac{\emptyset \mathrm{kA} + \mu\delta\bar{\rho}}{\mathrm{kA} + \delta\bar{\rho}} = \mu + \mathrm{mC}_e \tag{3}$$

where coefficient $m=k(\emptyset-\mu)$, and $C_e = A_g/F_{ng}$ can be associated with the cutting ability of the single grain. When A_g becomes bigger, more material will be removed, C_e is a coefficient of removal ability. Eq. 3 can be used for studying the friction coefficient, which reveals a linear relation between ε and C_e. It theoretically shows that the value of ε at $C_e=0$ is the friction coefficient μ where no cutting occurs and just the plastic deformation associated with plowing happens.

The theoretical model of the single grain test is not accurate since many parameters such as material pile-up and external sources such as vibration and machine stiffness are not considered in the model. Thus, a regression model was fit as a function of the average grain size, the cutting speed, and the depth of cut from the results of single-grain test. The unknown coefficients in the model are determined by minimizing the mean square error of the experimental results (least square method) [49]. The regression equation for the normal grain force can be accordingly expressed as:

$$F_{ng} = 4.65 \times 10^{-5} {d_g}^{1.36} {a_g}^{0.513} {v_c}^{-0.082} \tag{4}$$

where d_g is the average grain size (μm), a_g is the grain depth of cut in μm, and v_c is the cutting velocity in m/s. Eq. 4 implies that the cutting force increases when utilizing larger grains and depths of cut; and reduces with increasing the cutting velocity. It is valid for the boundary conditions set by the conducted scratch tests of titanium for the range of performed experimental parameters listed in Table 1. The regression latter reflects the dependency of the material properties on the strain-rate. According to this regression equation, the cutting conditions of each cutting grain can be expressed in the term of a normal cutting force. Through integration of the normal grain force components of individual grains in tool-workpiece contact zone of the actual grinding process, the total normal grinding force can be estimated. The tangential force component can be further obtained by applying the grinding force ratio (ratio of the tangential to the normal grinding force; assumed value of 0.65 for the titanium) [50].

Table 1. Process parameters for single-grain test [47]

Parameters	Values
Low cutting speed, v_c (m/min)	1.71
High cutting speed, v_c (m/s)	67, 90 and 120
Feed speed, v_{ft} (m/min)	1.71

3.2. Grinding tool modeling

The distribution of cutting grains over the surface of the grinding wheel is stochastic. Therefore, in case of a macro-grinding process, featuring a large grinding wheel, modeling the exact topography of the tool is impossible. One of the methods to model the grinding wheel topography is using the Probability Density Function (PDF). In this function, the shape parameters K and the scale parameter λ_g of the PDF can be defined according to the actual topography of the grinding wheel obtained from the confocal microscopy image as explained by Zahedi and Azarhoushang [51]. These parameters can be easily obtained via the Abbott curve from the software.

$$f_\Gamma(x) = \begin{cases} \dfrac{\lambda_g{}^K x^{(K-1)} e^{-\lambda_g x}}{\Gamma(K)} & x \geq 0 \\ 0 & x < 0 \end{cases} \tag{5}$$

where Γ is the Gama function.

In micro-grinding process, however, the diameter of the tool is small (in our case 2 mm), and the abrasive grains of the grinding tool can be modeled as distributed according to their real position on the actual grinding pin. For this purpose, the surface of the grinding pin was captured by a confocal microscope. Fig. 15 shows the confocal image of the actual topography of a vitrified-bonded diamond grinding tool (D46-C150).

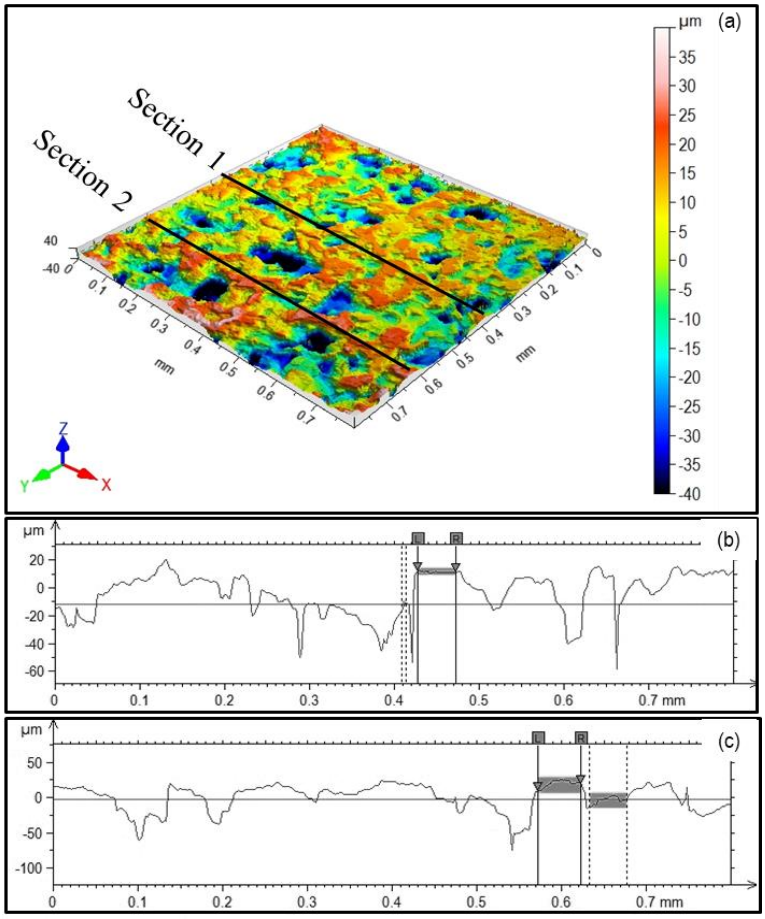

Fig. 15. a) Confocal picture from the grinding tool, b) Height profile of the Section 1, c) Profile of the Section 2

After taking the pictures, several sections were extracted, and the position and protrusion height distribution of each single grain were extracted and used to model the grinding tool (as illustrated in Fig. 15). The *y* direction defines the position of the grain in peripheral direction which can be defined from the position of section in Fig. 15-a. The position of the grain in the longitudinal direction along the tool axis can be obtained from the horizontal axes of Fig. 15-b. In order to ensure that the chosen grain (profile in Fig. 15-b) represents the real grain, the width of the profile has been measured. The grains are bonded over the surface of the grinding wheel and the measured area can be also the bound, which, in this case is vitrified. If the width of the profile (marked in Fig. 15-b and c) is around the grain size, the chosen profile is an actual abrasive grain. Finally, the protrusion height of each single grain can be measured from the vertical axes in Fig. 15-b and c.

Fig. 16 shows a section from the visualized grinding tool, modeled according to the actual position of the grains. The whole grinding tool surface is obtained by extending the modelled section of the wheel surface to its whole width and periphery. According to Shaw [52], it is assumed that the tips of the grains have a spherical shape. The grain diameter is also defined according to the grain size of the tool which is 45 µm.

3.3.Kinematics of the peripheral flank-surface grinding

The results of the single-grain scratch test can be extended to the aggregate cutting action of abrasive grains on the grinding tool surface through defining the distribution of the grains and the grain-workpiece interaction. By expressing the coordinates of the cutting grains (X_i, Y_i, Z_i) and the individual points on the workpiece surface (X_j, Y_j, Z_j) in a global coordinate system fixed at the workpiece, the grain-workpiece engagement can be characterized and interpreted according to the generated regression model. The engagement criteria of the i^{th} grain can be consequently expressed as:

$$(X_i - X_j)^2 + (Y_i - Y_j)^2 + (Z_i - Z_j)^2 < \left({}^{d_{gi}}/_{2}\right)^2 \tag{6}$$

where d_{gi} is the diameter of the i^{th} simulated grain. The equation expresses the instantaneous distance between the points on the workpiece surface and individual cutting grains. In the case of engagement (when Eq. 6 holds), the grinding force components and the workpiece surface topography are calculated according to the engagement depth, grain size and cutting velocity. The proposed procedure is applied to the all grains on the tool-workpiece contact zone at each time increment.

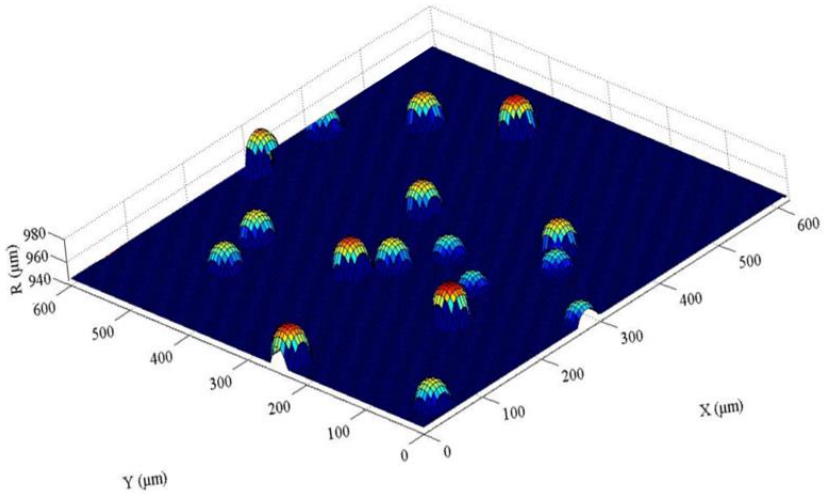

Fig. 16. Simulated grains on the projected surface of grinding pin

The proposed model makes it possible to consider the effects of the individual grain regarding the time-dependent workpiece surface topography modified by previous cutting grain. Therefore, after the calculation of the grain engagements (Eq. 6) and corresponding forces, the workpiece surface is also modified accordingly. This procedure results in the generation of the workpiece surface profile influenced by all cutting grains throughout the grinding process. A Matlab code was specifically generated for the modelling of tool surface and the time-dependent simulation of the grinding process (force and workpiece surface).

4. Experimental work

To validate the simulate results a set of experimental tests were performed, and simulation was modified based on the experimental results.in this section, a detail description of the experimental procedure and measurement is provided.

4.1. Micro-grinding experiment:

One of the main difficulties in performing micro-machining experiments is the availability of appropriate machine tool that can be used for implementing micro-machining processes and specially to utilize a tool-based micro-machining for fabrication of components at the required scale. Some requirements that high/ultra-precision machines over a range of applications shall have is listed as following [1]:

- High dimensional precision better than a few microns.
- Accurate geometrical form better than 100 nm departure from flatness or roundness.
- Good surface finish, in the range of 10 – 100 nm Ra.
- High static stiffness.
- Low thermal distortion.
- Low motion errors.
- High damping or dynamic stiffness.
- Facilitate measurement of fabricated products on-machine.
- Avoidance of chatter vibration.
- Good tooling and clamping to achieve minimum tool run-out and minimum errors from re-clamping.
- Specialized precision motion control system.

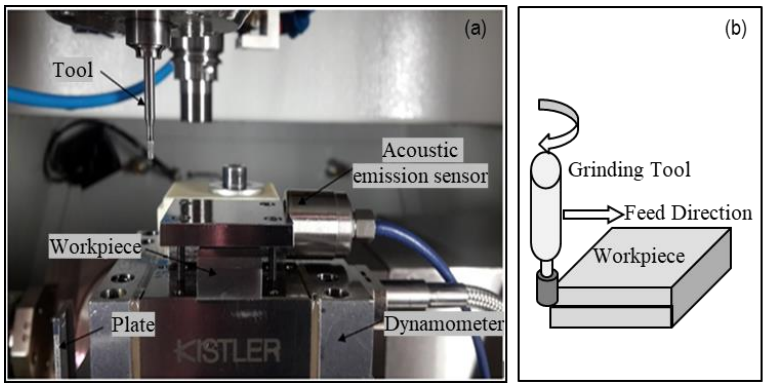

Fig. 17. a) Experimental setup, b) schematic of the grinding process

In this study a high precision CNC machining center (Kern Pyramid-Nano) was used in order to perform the micro-grinding tests with high rotational speed and accuracy. Thanks to its hydrostatic drives and guides, the machine suffers virtually no wear of its linear axes. This means the quality and precision of all axes remain constant over extremely long-time period. In conjunction with KERN's proprietary thermal management system, it is possible to have a precise tool position at any time. The machine consists of two spindles one with hydrostatic bearing and the other with mechanical bearing. The hydrostatic bearing enables to achieve a high rotational speed; up to 160000 1/min (Fig. 17-a). A peripheral flank-grinding operation has been chosen to perform the micro-grinding experiments. In this method the peripheral

surface of the grinding wheel removes the material from the surface of the titanium material which is shown in Fig. 17-b. Ti4V6Al titanium alloy in the form of a block with the dimensions of 30x20x10 mm was used as the test material.

4.2. Micro-grinding forces

The tools in micro-cutting operation are mostly rotating with high rotational speeds (more than 100000 rpm), resulting in high excitation frequency. Therefore, it is nearly impossible to measure the cutting forces within a wide frequency range because of the interference of the excitation frequency with the natural frequency of the used dynamometers. Finding a dynamometer which its lowest eigenfrequency exceeds the excitation frequency by more than a factor 3 is difficult. This factor enables the dynamometer to accurately measure the process forces in micro-machining operations [53]. Transchel et al. [53] showed that the commercial Kistler type 9256 dynamometer is suitable to measure the micro-cutting forces, Therefore, the micro-grinding forces presented in this study were measured using a Kistler type 9256C2 three-component dynamometer shown in Fig. 17. The dynamometer was connected to the amplifier type 5015 and the forces were recorded via a LabView software.

4.3. The surface roughness

The generated surface roughness in this study was measured using a tactile surface roughness tester (Hommel-Werke model T-1000) shown in Fig. 18-a. A confocal microscope (μsurf mobile plus) was used to obtain the confocal pictures from the topography of the ground surface. The surface roughness measurements were taken perpendicular to the grinding direction at three positions: at the beginning, at the middle, and at the end of the grinding path.

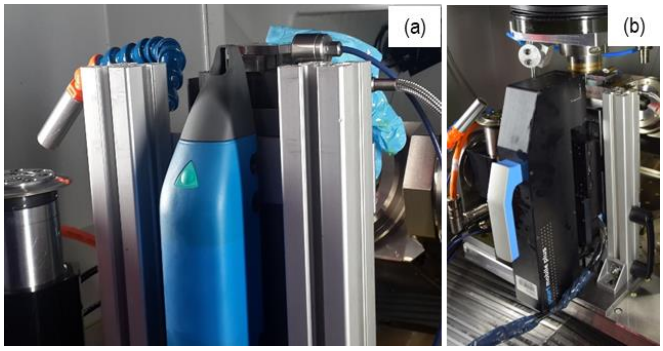

Fig. 18. Measurement setup for the surface roughness a) using the tactile surface roughness tester, b) using the confocal microscope

4.4. Chip loading

A digital microscope (Keyence VHX-100) was mounted in the machine to take pictures of the grinding pin after the dressing (prior to grinding), and after the grinding. The grinding tool was dressed, and after the dressing process, the periphery of the grinding tool was marked at three different regions (0, 120, and 270 degree). Prior to the grinding three images from each marked area were taken using the digital microscope. The pictures were stored, and the relevant grinding test was performed. After the grinding test, the surface of the grinding tool was captured from the same marked positions. The taken pictures after and prior to the grinding tests were compared to calculate the amount of the chip loading over the surface of the grinding

tool. This procedure was repeated for all the trials. Accordingly, the chip loading as the results of different grinding and dressing parameters was determined and compared in relative terms.

4.5. Dressing

The micro-topography of grinding tools, which is greatly affected by the dressing process, plays a key role in the performance of the grinding process. It can influence not only the grinding forces and temperature, but also the surface finish and integrity [54]. The grinding tool micro-topography undergoes several changes during the grinding process due to the tool wear – causing variation in grinding forces and surface roughness [55]. Hence, a periodic dressing of the grinding tool is needed to maintain (or reproduce) the initial micro-topography of the tool and remove or reduce the level of tool run-out. Accordingly, the dressing process can be considered as an integral part of the grinding process.

Fig. 19. The setup for the digital microscope

Several researchers investigated the effects of the dressing parameters on the macro-grinding process. Rasifard [56] studied the effect of the ultrasonic-assisted dressing (UAD) of vitrified-bonded cBN grinding wheels with diamond form rollers and showed that the wear of the grinding wheel can be reduced up to 50 % when using the UAD. Daneshi et al [57] studied the effect of dressing parameters on internal cylindrical grinding and suggested that after the dressing and prior to grinding, the wheel should be sharpened or relatively low feed rates should be utilized when grinding the first part. Malkin and Murray [58,59] studied the mechanics of the dressing process and showed that rougher grinding tool surface induces lower grinding forces and rougher surface finished. Linke [60] presented a model for predicting the grinding wheel topography after dressing with different parameters. She also used this model to predict the dressing forces [61]. Linke and Klocke [62] measured the dressing temperature generated in the contact zone between the grinding tool and the dresser. They observed significant wear of the diamond dressing tools after the dressing. Saad et al [63] investigated the effect of dressing parameters on the ground surface roughness. Azarhoushang and Rasifard [54] presented the most important variants of the dressing process for different types of grinding tool bonds such as synthetic resin, metal and vitrified. All the mentioned studies utilized relatively low dressing overlap ratios, U_d, (generally U_d is smaller than 8) and showed that higher U_d normally induce very high grinding forces and temperatures, and hence, lead to a poor surface integrity of the workpiece. The very recent research on the fundamentals of diamond-wheel conditioning postulates hitherto unknown diamond removal mechanisms and postulates new parameters to analytically model the process [54,64].

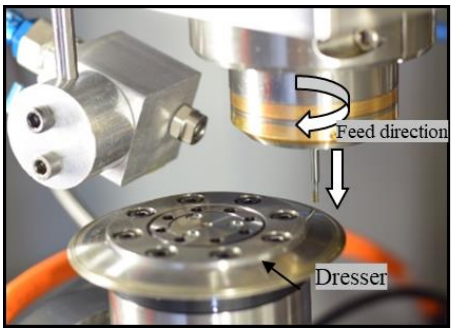

Fig. 20. Dressing setup

In this study, the grinding pin was dressed using a diamond dressing roller with the diameter of 100 mm. Oil was utilized as the grinding fluid. The dressing tests were carried out at different dressing-speed ratios (q_d), and dressing-overlap ratios (U_d). The dressing-speed ratio is the ratio of the peripheral speed of the roller dresser to the peripheral speed of the micro-grinding pin following by a sign. The speed directions of the dresser and the tool in the contact zone can be defined using this sign. If the speed directions are the same, the dressing is called down dressing designated as positive. If the speed directions are opposite to each other, the dressing speed ratio is negative, which is called up dressing. The dressing overlap ratio is the ratio of the engagement width of the dresser and the axial dressing feed of the dresser per grinding tool revolution. In practice, this ratio is often extracted from the active width of the dresser [65]. The dressing overlap ratio is calculated as:

$$U_d = \frac{\sqrt{(8 r_{pd} a_{ed})}}{f_{ad}} \tag{7}$$

where a_{ed} is the dressing depth of cut, r_{pd} is the radius of the dressing tool and fad is the axial feed ($f_{ad} = v_{fad}/n_s$; where n_s is the rotational speed of the grinding pin). Here, we are assuming that the width of cut equals the active width of the dressing tool [66]. In macro-dressing, the overlap ratio typically ranges between 2 and 8. In micro-dressing since the diameter of the tool is very small (i.e. 2 mm); the rotational speed of the tool should be very high to achieve required cutting speed v_c values (e.g. almost 100000 1/min for the cutting speed of 10 m/s). Consequently, since extremely high v_{fad} is needed to achieve U_d values smaller than 10, the low values of U_d are not applicable in micro-grinding. As a result, much higher values of dressing overlap ratios U_d were used in this study, and the effects of these very high U_d values on grinding performance are studied for the first time.

Table 2. Process Parameters

Grinding Parameters	Values
Cutting Speed, v_c (m/s)	6, 10, 12 and 14
Feed Rate, v_{ft} (mm/min)	200, 500 and 1000
Depth of Cut, a_e (µm)	4, 7 and 10
Width of Cut (mm)	2.5
Dressing Parameters	**Values**
Dressing Depth, a_{ed} (µm)	2
Dressing Speed Ratio, q_d	-0.4, +0.4 and +0.8
Dressing Overlap Ratio, U_d	45, 90, 270, 305, 910, 1830

The process parameters including the dressing parameters are listed in Table 2. the corresponding dressing feed rates for overlap ratios of 45, 90, 270, 305, 910, and 1830 at the cutting speed of 10 m/s are 2000, 1000, 350, 300, 100, and 50 mm/min, respectively.

5. Results and discussions

5.1. Micro-grinding forces

5.1.1. The effect of cutting speed

This section presents the results of micro-grinding forces and surface roughness obtained from the simulation and experiments. The effects of the process parameters as well as dressing parameters are presented and discussed. The experimental and simulated normal and tangential grinding forces versus different cutting speeds are presented in Fig. 21. Both simulated and experimental forces follow the same trend and are matched qualitatively. Increasing the cutting speed decreased the grinding forces, as expected. This could be because of the changes in the kinematic energy and the impact force of each single abrasive grain with increasing the cutting speed. Increasing the cutting speed reduces the number of kinematic cutting edges and the mean uncut chip thickness of each active grain [67].

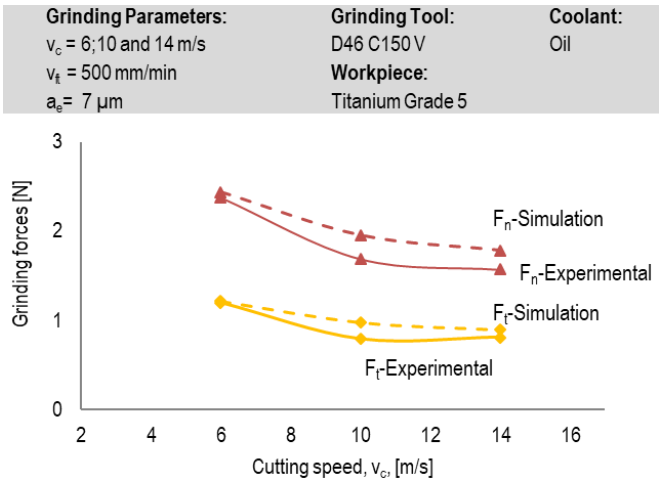

Fig. 21. Grinding forces versus cutting speed.

The number of kinematic cutting edges can be defined by Eq. 8, where L_n is the spacing along the tool surface from the prospective cutting point to the proceeding active one, δ_n is the protrusion deference between the cutting points of n and n-1, v_w is the workpiece velocity, and d_e is the equivalent diameter of the grinding tool [68]. Decreasing the v_w/v_c ratio decreases the number of kinematic cutting edges owing to the reduction of the number abrasive grains which do not come into the contact with the workpiece surface. The uncut chip thickness (h_m) can be defined according to Eq. 9 [68]. However, increasing the L increases the uncut chip thickness, its effect is smaller than the v_w/v_c ratio [68]. Therefore, increasing the cutting speed decreases both the uncut chip thickness and the number of kinematic cutting edges. Hence, the grinding forces, which are acting on each active grain, are decreased – resulting to lower grinding forces. In Fig. 21, the simulation results for tangential and normal forces were accurate within the total error of 11.5 and 10.5 percent, respectively.

$$\frac{\delta_n}{L_n} > 2\left(\frac{v_w}{v_c}\right)\left(\frac{a_e}{d_e}\right)^{1/2} \tag{8}$$

$$h_m = 2L\left(\frac{v_w}{v_c}\right)\left(\frac{a_e}{d_e}\right)^{1/2} \tag{9}$$

5.1.2. The effect of depth of cut

Fig. 22 shows the tangential and normal grinding forces versus the depth of cut. Both tangential and normal forces increased with increasing the depth of cut. The same trend can be seen for simulated forces. Higher depth of cut causes higher material removal rate and thicker uncut chip thickness — resulting in higher normal and tangential forces. Additionally, increasing the depth of cut increases the contact length of the grinding tool with the workpiece and the number of the momentarily engaged cutting edges — inducing higher grinding forces [69]. According to the experimental results, the grinding force ratio lies within 10% of the assumed value in the modelling. Therefore, the assumption of a constant force ratio could be acceptable for a specific material and defined range of the grinding conditions.

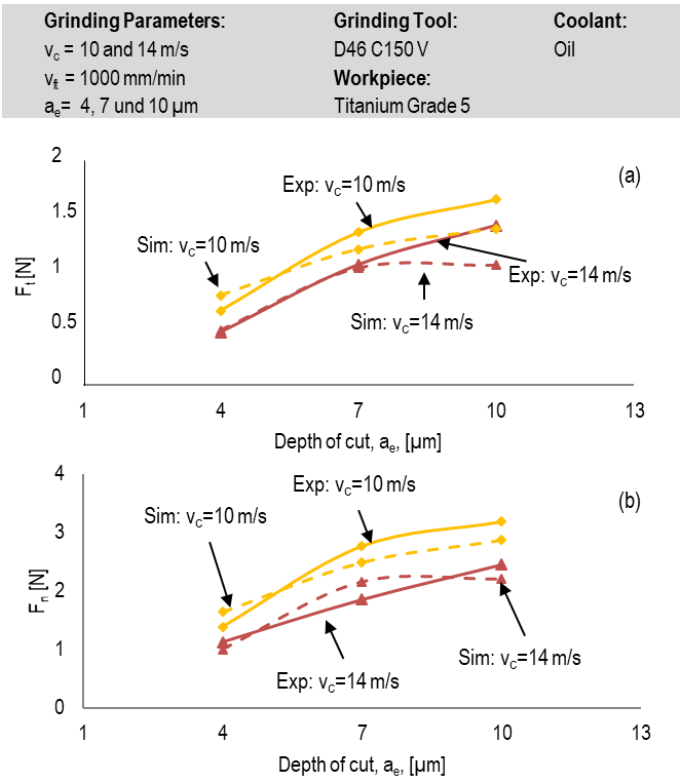

Fig. 22. Grinding forces versus depth of cut: a) tangential force; b) normal force

Although, the prediction of the tangential force is qualitatively matched with those in the experimental study by increasing the depth of cut, the predictions are more accurate at the smaller depths of cut. The variation in the predicted grinding forces can be associated with the following causes:

- During the grinding process, the number of active cutting edges changes due to the grain breakage and pull-out. Hence, different active grains are available at different height levels – inducing different force values.
- The actual grains are normally sharper than the assumed spheres.
- In modeling process, it was assumed that the grains are ideally spherical. However, in the real grinding tool they have different shapes.
- The wear of active grains in the real grinding process increases at higher depths of cut. Hence the grit protrusion will be reduced and become smaller than the simulated grit protrusion.

5.1.3. The effect of dressing overlap ratio

According to Fig. 23, high dressing overlap ratios (achieved by reducing the dressing feed) increased the cutting forces. The micro-topography of the grinding tool is affected by changing the dressing overlap ratio (Eq. 2), which gives the relationship between the theoretical grinding tool surface roughness, R_{ts}, and the dressing overlap ratio (Eq. 10) [70].

$$R_{ts} = \frac{a_{ed}}{U_d^2} \tag{10}$$

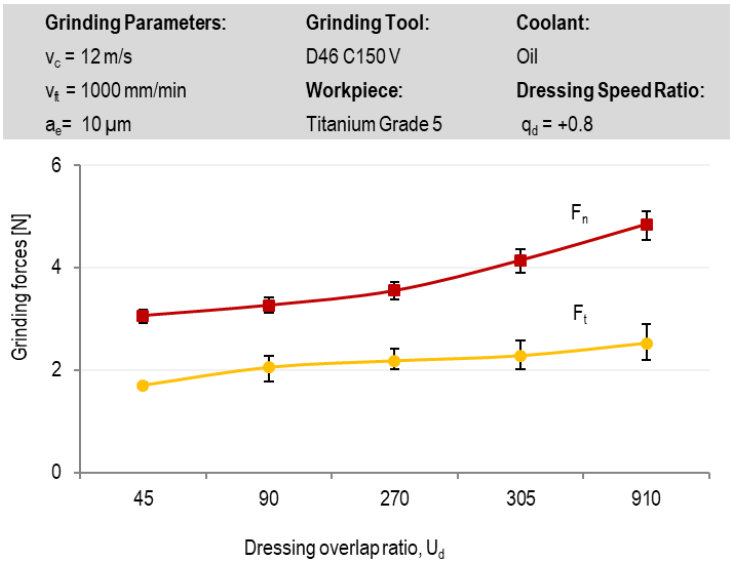

Fig. 23. Grinding forces F_n and F_t versus the dressing overlap ratio, U_d

Here, the higher U_d values lead to a finer micro-topography of the grinding tool – resulting in an increased number of static and kinematic cutting edges, rising the amount of rubbing and plowing in grinding, which explains the observed rise in the grinding forces. On the other hand, higher dressing overlap ratios reduce the proportion of the grit break-out by dressing [61]. This phenomenon can be explained with reduced dressing forces when increasing the dressing overlap ratio [71]. High dressing forces (which occur at lower dressing overlap ratios), lead to an aggressive dressing of the grinding pin. Hence, the grain tips may be broadly fractured and coarse. In contrast, it has been shown that the grain tips are much more flattened when the dressing feed rate is low (i.e. at high U_d values) [58]. Therefore, the surface of the grinding tool is rougher (and the grains become sharper) when using higher dressing feed rates; hence the sharper the grains, the lower the cutting forces. Both normal and tangential forces F_n and F_t increase with bigger wear-flat area on the grains, as estimated by Eqs. 11 and 12 below.

$$F_t = F_{t,c} + \mu \bar{p} b (d_e a_e)^{1/2} A \tag{11}$$

$$F_n = F_{n,c} + \bar{p} A_a (d_e a_e)^{1/2} A \tag{12}$$

$$A_a = b (d_e a_e)^{1/2} A \tag{13}$$

Here, $F_{t,c}$ and $F_{n,c}$ are the tangential and normal forces for cutting, $\bar{p}$ is a constant average of contact stress, μ is the friction coefficient, A is the fraction of the tool surface which consists the wear flat, A_a is the actual contact area between the wear flat and the workpiece (calculated by Eq. 13), b is the grinding width, d_e is the equivalent diameter (in surface grinding d_e is equal to pin diameter) and a_e is the depth of cut. The lower the value of R_{ts}, the higher the flat area, A.

The normal micro-grinding force starts at about 3 N for the U_d=45 and increases up-to 5 N for U_d=910, i.e. approximately a 70% increase. A reason for this increase could be the dressing temperature; since lower dressing feeds reduce the average dressing temperatures [62]. The friction between the dresser and the grinding tool could be reduced, causing lower fracture of the abrasive grains.

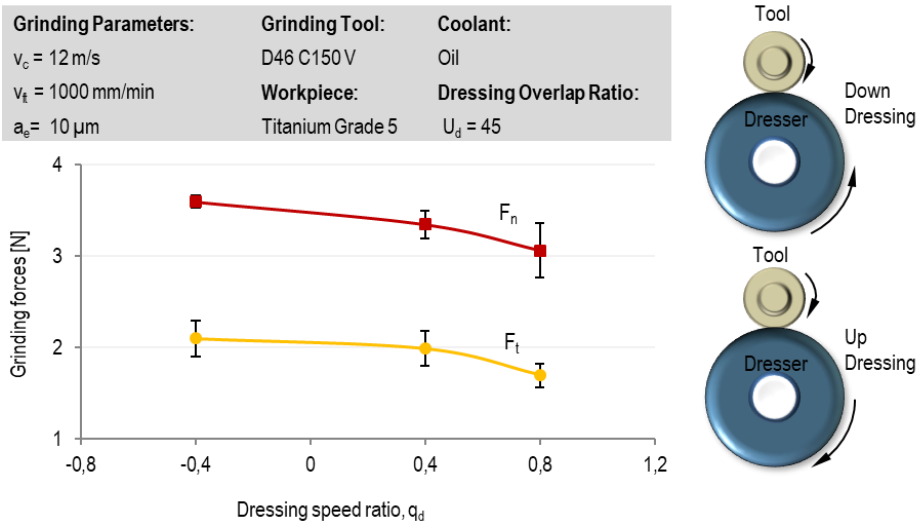

Fig. 24. Grinding forces F_n and F_t versus the dressing speed ratio, q_d

5.1.4. The effect of dressing speed ratio

In rotary dressing, the grinding tool and the dressing roll engage against each other in a rotational movement. The used speeds and the rotational directions, determine the dressing-speed ratio, q_d, which has a significant effect on the dressing process. The speed ratio is therefore another dressing parameter which must be considered when generating the micro-topography of the grinding tool. As such, q_d, affects the dressing forces [60] and can be calculated as:

$$q_d = \frac{v_{cd}}{v_c} \tag{14}$$

where v_{cd} is the dressing-roller cutting speed. Rotary dressing can be categorized into two different processes, anti-directional up-dressing ($q_d < 0$) and uni-directional down-dressing ($q_d > 0$). In most operations, the common dressing speed ratios vary between -0.8 and +0.8. The grinding forces versus dressing speed ratios are shown in Fig. 24. Here we can observe that increasing the speed ratio from -0.4 to +0.8 decreases the grinding forces noticeably.

An increase in the speed ratio, q_d, increases the dressing aggressiveness, leading to more grit breakage and/or break-out from the surface of the grinding tool. Moreover, the effective roughness of the grinding tool is higher when employing down-dressing, compared to the up-dressing [57,67,72]. In contrast, the contact length of the dresser-grinding tool is much larger in up-dressing compared to down-dressing, causing more wear-flats and finer surface roughness of the grinding tool which result in higher grinding forces. This can be schematically explained on Fig. 25-a, which illustrates the path of a diamond grain of the dresser over the surface of the grinding pin.

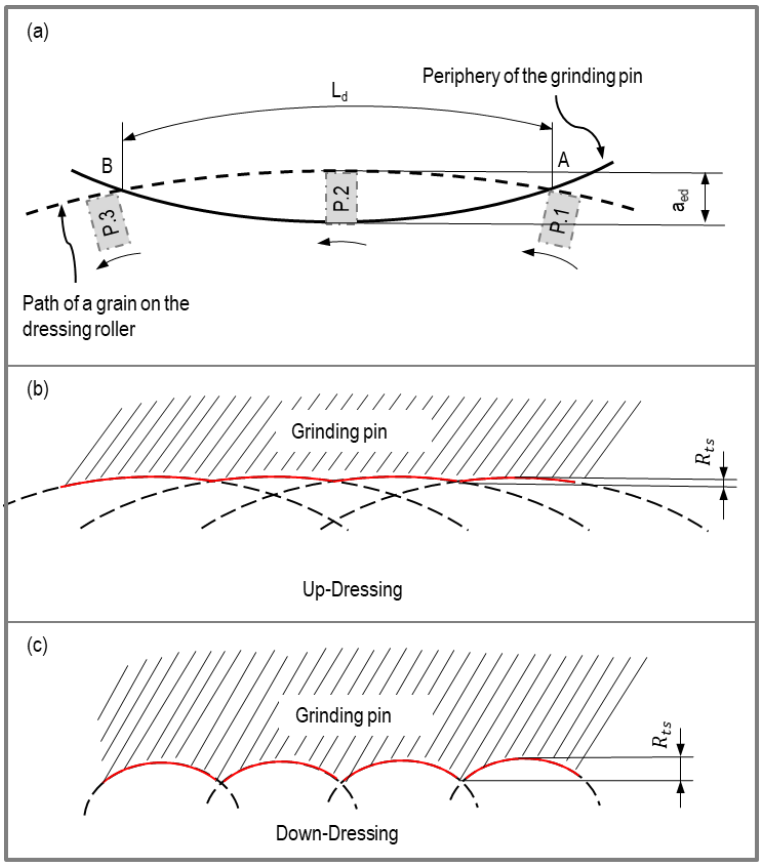

Fig. 25. a) Illustration of the dressing path, b) generated path on the grinding tool surface with up-dressing method, and c) generated path on the grinding tool surface with down-dressing method

The dressing process starts at the point A (P.1) and ends at the point B (P.3), generating the dressing path L_d. The diamond grain reaches the maximum engagement depth of a_{ed} with the grinding tool at the point P.2. For up-dressing, the duration of the grain moving from P.1 to P.3 can be calculated as [73]:

$$dt = (t_3 - t_1) = \frac{dl_{(P.1\ to\ P.3)}}{v_{cd}} \tag{15}$$

$$t_3 - t_1 = \frac{L_d}{v_{cd}} \tag{16}$$

where t_3 is the time instant at which the diamond grain exits the grinding wheel (at position P.3) and L_d is the length of the dressing-grain path from P.1 to P.3. For both up- and down-dressing, the dressing path generated on the surface of the grinding tool (L_s) can be calculated using:

$$L_{s(P.1\ to\ P.3)} = (t_3 - t_1).(v_c - v_{cd}) \tag{17}$$

Combining Eqs. 14-17, while neglecting the size of the diamond grain the L_s can be expressed as: [73]:

$$(-1 \le q_d \le +1):\ L_s = \left|\left(\frac{1}{q_d} - 1\right) \cdot L_d\right| \tag{18}$$

According to Eq. 18, the contact length of the dresser with the micro-grinding pin increases when changing the dressing method from down- to up-dressing. As shown in Fig. 25-b and c, changing the contact length and contact geometry both affect the theoretical roughness of the grinding pin. The obtained topography, shown as red patterns in Fig. 25-b and c, reveals the generated profile on the grinding pin by two different dressing kinematics. In the up-dressing, the generated paths on the grinding pin overlap with each other since the contact length is larger (i.e. the radius is bigger). Therefore, the peak-to-valley height is reduced here, leading to a smoother micro-topography of the grinding tool.

5.2. Surface roughness

5.2.1. The effect of depth of cut

The surface roughness measurements have more scatter compared to the measured grinding forces. This is due to inherent higher variations in surface-roughness measurements, but also due to the fact that the measurements were done using a portable device in the machine after each grinding test. Vibrations and temperature changes could also cause higher variations.

Fig. 26. shows the simulated and experimental values of the surface roughness versus different depth of cuts. In both simulation and experiment, increasing the depth of cut resulted in the rougher surface finish. As it can be seen in Fig. 26, the surface roughness values, predicted by the simulation method, follow the same trend as the experimental values.

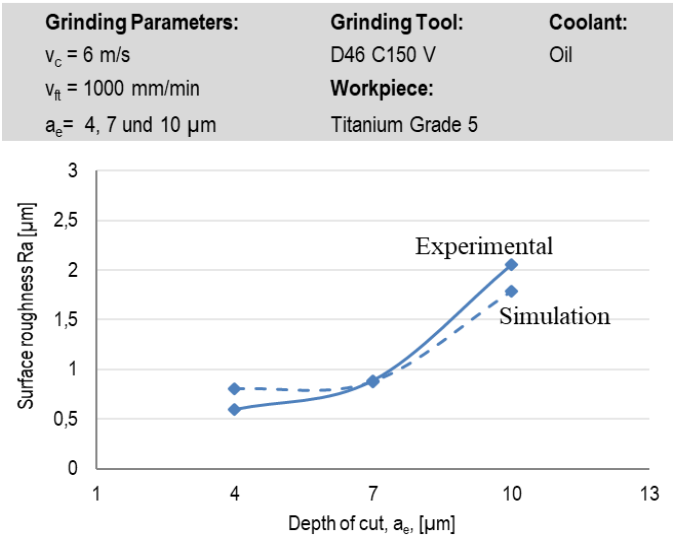

Fig. 26. Surface roughness versus depth of cut, a_e

Increasing the depth of cut increases the number of kinematic cutting edges and the mean uncut chip thickness of each active grain (Eqs. 7 and 9), therefore it leads to higher values of the surface roughness [68]. On the other hand, Increasing the depth of cut increases the grinding forces, consequently increases the stress on the finished surface which causes higher vibration and rougher surface roughness.

5.2.2. The effect of feed rate

The influence of the grinding feed rate on the surface roughness at the cutting speed of 14m/s has been shown in Fig. 27. The grinding feed rate has a negligible effect on the surface roughness. Although the surface roughness predicted by the simulation are finer than those obtained from the experimental study at the cutting speed of 14m/s, the trend of the roughness changes with varying the feed rate. The differences between the simulated and real surface roughness, seen in Fig. 27, can be due to the unavoidable vibration in the grinding process by using the cutting speed of 14m/s. The tool vibration is one of the influential factors which may significantly influence the surface quality. The very small diameter of the tool along with its high rotational speed causes the tool vibration which has been neglected in the simulation [74].

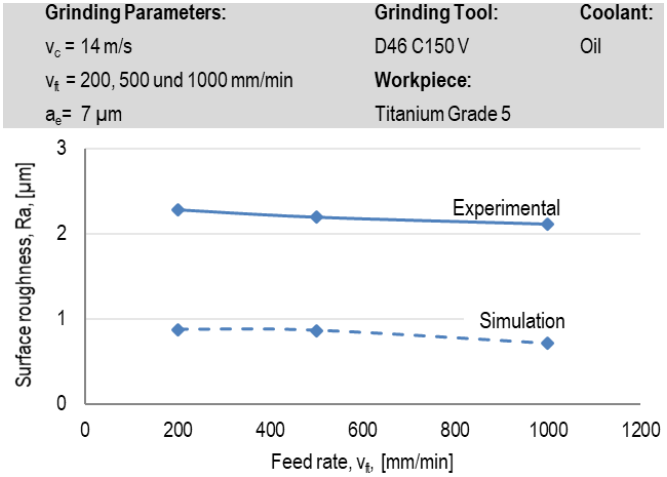

Fig. 27. Surface roughness versus feed rate, v_{ft}

The simulation results were matched with the experimental results in greater degree at the cutting speed of 6m/s (Fig. 26), rather than the higher cutting speed (14 m/s) as seen in Fig. 27. For instant, the predicted surface roughness at the cutting speed of 6 m/s, feed rate 100 mm/min, and depth of cut of 7 µm was similar to the real surface roughness (Fig. 26). However, changing the cutting speed from 6 to 14, not only changed the real surface roughness from Ra=0.89 to Ra=2.2, but also the simulated surface roughness was considerably different from that in the real situation at the cutting speed of 14 m/s. As known in the macro-grinding operations, increasing the cutting speed causes finer surface roughness because of the smaller chip thickness. With comparing Fig. 26 and 27, the simulation model predicted a finer surface roughness with increasing the cutting speed from 6 to 14m/s due to the smaller chip thickness. This does not agree with the experimental results in these figures since the tool diameter is very small and tool vibration occurs at the high rotational speeds which is neglected in the simulation process.

5.2.3. The effect of cutting speed

The surface roughness increased with rising the cutting speed in micro-grinding (Fig. 28). The same behavior was also reported by Li et al [75]. The surface roughness parameter, R_z is constantly rising with increasing the grinding cutting speed. In case of R_a, there is no significant

change in the roughness when increasing the cutting speed from 6 to 10 m/s. Nevertheless, the R_a increased slightly at the cutting speed of 14 m/s.

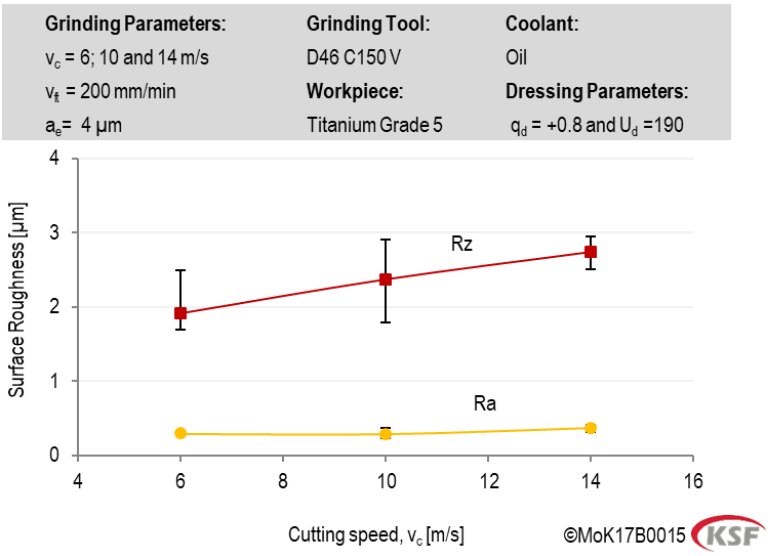

Fig. 28. Surface roughness *Ra* and *Rz* versus the cutting speed, v_c

These observations are important to consider since in conventional macro-grinding an increase in the cutting speed improves the surface roughness [76]. This well-known trend in macro-grinding can be explained by the basic of uncut chip thickness [67] model, which is explained in section 5.1 In micro-grinding, the diameter of the tool is very small – resulting in a high tool-length to diameter ratio. Hence, the grinding tool acts as a flexible cantilever beam, and the tangential grinding force F_t (acting radially on the tool) causes the tool deflection parallel to the uncut chip thickness [77]. While the grinding tool is rotating with a high rotational frequency during the process, the deflection of the tool causes undesirable lateral vibrations [78]. These vibrations at higher cutting speeds deteriorate the surface roughness. This phenomenon is not in accordance with the conventional understanding of the effect of the cutting speed in the grinding process. Normally, higher cutting speed improves the surface roughness in grinding process. However, the existed vibrations at higher cutting speeds in micro-grinding process can be predominated to the desired effect of the cutting speed and deteriorate the surface roughness.

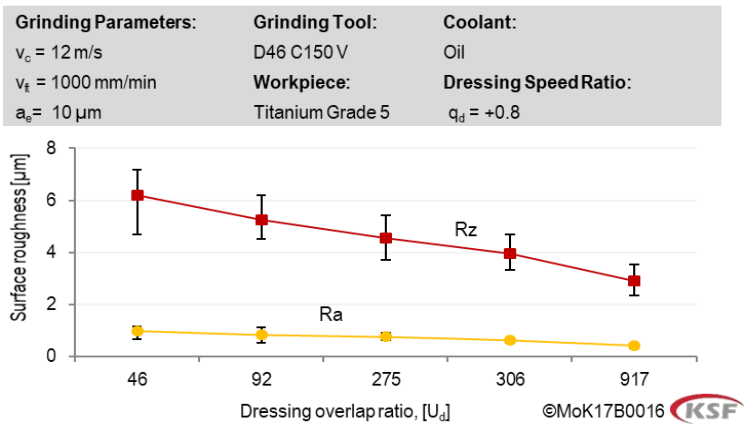

Fig. 29. Surface roughness *Ra* and *Rz* versus dressing overlap ratio U_d

5.2.4. The effect of dressing overlap ratio

To investigate the relation between the dressing overlap ratio, U_d, and the surface roughness, an aggressive grinding (i.e. grinding with a high material removal rate) was chosen. Here, the surface roughness improves by increasing the overlap ratio, as shown in Fig. 29. The observed surface roughness improvement is up to 60%, when increasing the dressing overlap ratio from 45 to 910. As already explained – higher dressing overlap ratios lead to a finer micro-topography of the grinding tool, reducing the surface roughness of the ground workpiece.

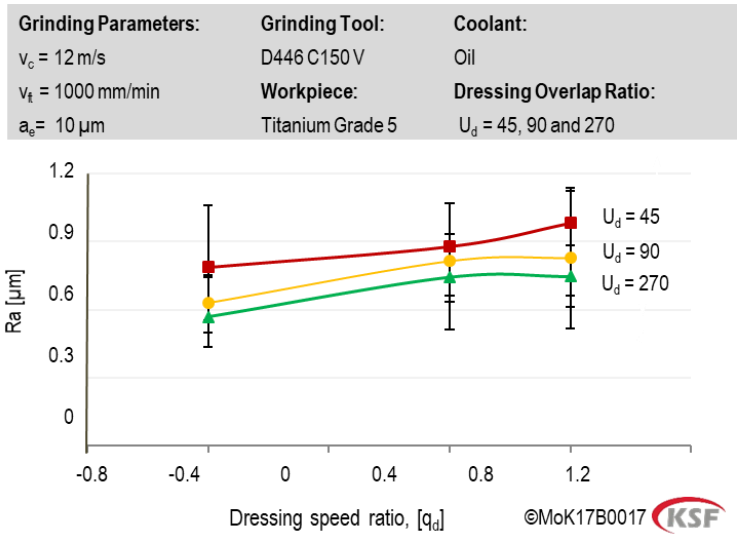

Fig. 30. Surface roughness, *Ra*, versus dressing speed ratio

5.2.5. The effect of dressing speed ratio

The relation between the surface roughness and the dressing speed ratio is shown in Fig. 30. Here it can be seen that the surface roughness increases when shifting from up-dressing to down-dressing. The theoretical roughness of the grinding tool increases with the dressing speed ratio, where higher tool roughness induces a rougher ground surface.

The micro-topography of the grinding pins is shown in Fig. 31. It is clear from the micro-graphs that the topography of the grinding pin is influenced by either the dressing overlap ratio (Fig. 31 (a) to (c)), or the dressing speed ratio (Fig. 31 (a) and (d)). Up-dressing induces a more even tool surface – with almost a constant grain protrusion from the bond – giving a finer micro-topography of the tool [66,79]; since many grains can be easily detected and seen in the Fig. 31 (d), compared to the Fig. 31 (a). In up-dressing, the vectors of the peripheral speed of grinding tool and the dresser have different directions which means longer contact time in comparison with the down dressing (positive quantities of the dressing speed ratio) as it has been explained in Fig. 25.

In grinding, the chip loading can be divided into two categories, (a) chip nesting and (b) welded-clogging [80]. Chip nests are formed when the chips tend to stick in the tools' pores (spaces between grits). The welded clogging occurs when the chips are cold-welded to the grains. The chip nests are not very critical for the grinding process, since they mainly do not detrimentally affect the ground surface quality and can be removed easily with proper cooling and lubrication. The grinding pins, up-dressed with the dressing overlap ratios smaller than 90

were subjected mainly to the welded clogging (Fig. 31(a) and (b)), whereas, the up-dressed pins experienced loading in the form of chip nests during the grinding process (Fig. 31 (d)).

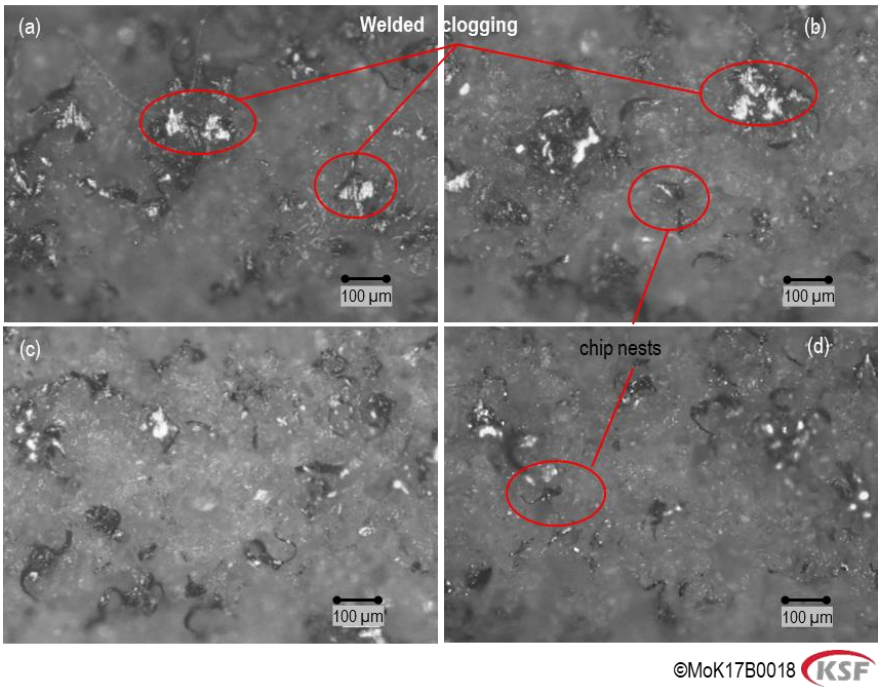

Fig. 31. Chip loading of the grinding pin in different dressing conditions after the grinding process (a_e = 10 µm; v_{ft} = 1000 mm/min; v_c = 12 m/s): a) q_d = +0.4 and U_d = 45; b) q_d = +0.4 and U_d = 90; c) q_d = +0.4 and U_d = 270; d) q_d = -0.4 and U_d = 45

Fig. 32 shows the ground surfaces when employing different dressing speed ratios, q_d. It is clear from the microscopic images that changing the dressing speed ratio affects the surface quality. Although, the grinding forces were higher when using up-dressing, the surface damage is much lower than in down-dressing. This may be associated with the flatness of the grinding tool surface. As mentioned previously, the down-dressing induces a rougher effective roughness of the grinding pin. Since there is a limited amount of cutting edges available on the grinding-pin surface, a rougher surface means that the material removal takes place by a few active cutting edges. This leads to a much higher chip thickness – cutting loads on individual grains, increasing the wear rate of the active cutting edges and the cold-welded clogging of these few active cutting edges (Fig. 31 (a) and (b)). Higher wear of active cutting grains in conjunction with clogging of the micro-grinding pin deteriorate the surface quality as revealed in Fig. 32. Consequently, the ground surface integrity is degraded during grinding, subjected to cracks and loading of the chips to the ground surface.

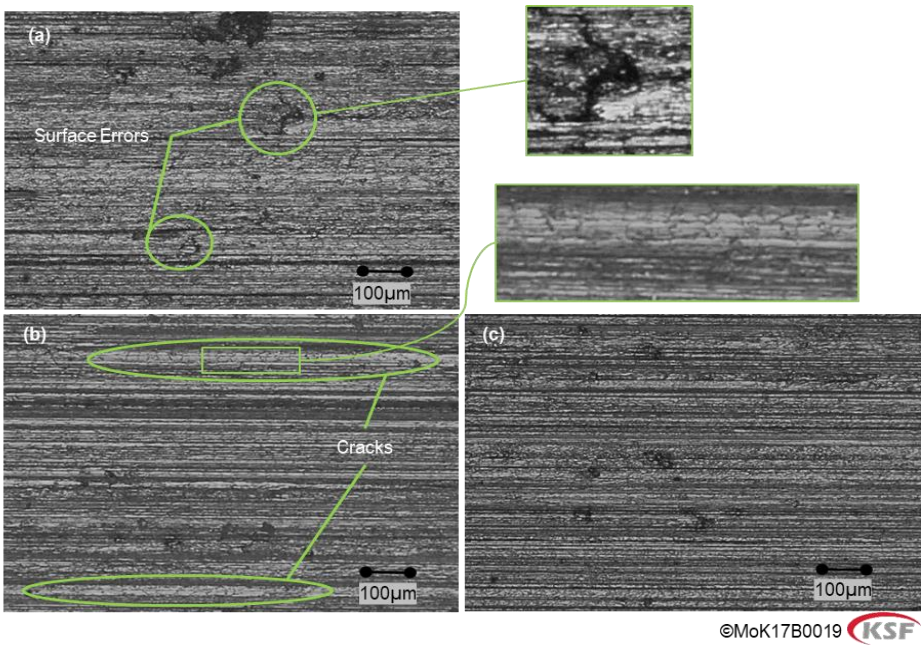

Fig. 32. The quality of the ground surfaces at different dressing parameters (a_e = 10 µm; v_{ft} = 1000 mm/min; v_c = 12 m/s; U_d = 270): a) q_d = +0.8, b) q_d = +0.4, and c) q_d = -0.4

Based on the analysis of the research results, the best grinding result, validated experimentally, generated a surface roughness of R_a = 0.25 µm. The following grinding and dressing parameters were utilized for achieving this surface finish: v_c = 10 m/s, a_e = 4 µm, q_d = 0.8, v_{ft} = 200 mm/min, and U_d = 910. The related confocal picture of the ground surface is shown in Fig. 33. Here, we can observe an almost uniform surface, obtained when using appropriate grinding and dressing parameters.

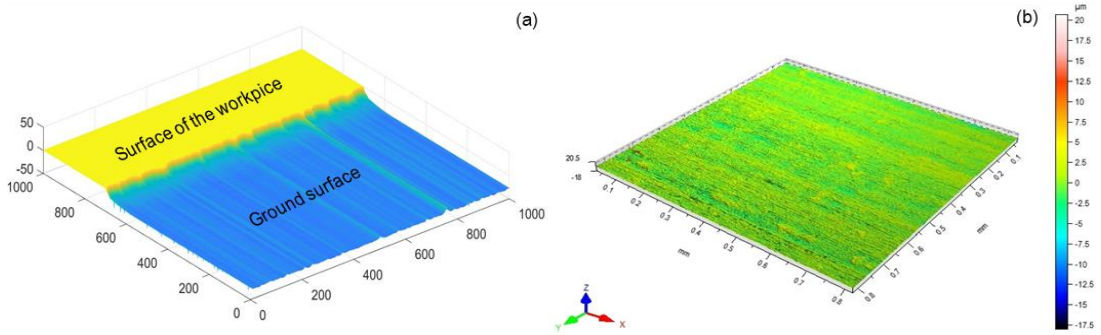

Fig. 33. a) Pattern of the ground surface obtained from the simulation model, b) confocal picture of a ground surface

6. Conclusions

6.1. Paper I

- The dressing overlap ratio and the speed ratio are influential factors, affecting surface roughness and grinding forces in micro-grinding of titanium Ti-6Al-4V.
- Increasing the dressing overlap ratios (U_d up to 1830) reduced the surface roughness but led to approximately 70% higher cutting forces because of finer surface of the grinding-pin.

- The employment of extremely high dressing overlap ratios in an up-dressing method, improved the surface finish. This is explained by less chip loading. As in conventional dressing, the down-dressing of micro-grinding pins caused rougher surface finish and lower grinding forces compared to up-dressing.
- The grinding forces could be reduced up-to 40% by increasing the cutting speed from 6 to 14 m/s, however, led to an increase in the surface roughness. In the term of accuracy, it can be an important result for the industry.
- Higher values of the dressing overlap ratio reduced the chip cold-welding on the abrasive grains and led to less loading of the tool in form of chip nests. Welded clogging of the grinding pin at lower values of U_d deteriorated the surface quality and increased the surface roughness of the ground surface.
- A uniform surface with almost no cold-welded clogging was observed when employing up-dressing. The up-dressing was improved via increasing the dressing overlap ratio from 45 to 917, resulting a significant reduction in surface roughness of Rz from 6.19 to 2.88 µm and Ra from 0.98 to 0.4 µm.
- The results showed that the surface quality, grinding forces, and chip loading of the grinding tool are highly affected by the dressing parameters and can be optimized by changing U_d and q_d. Hence the new insights regarding the influence of extremely high values of U_d (which are not used in conventional dressing of (large) grinding wheels) in micro-grinding have an important industrial relevance. Achieving a desired surface roughness is one the biggest challenges in the industry and the outcomes of the research are highly useful not only in the term of surface quality, but also accuracy for workshop practice. Future research necessitates the use of additional dressing parameters.

6.2. Paper II

- The developed model enabled the prediction of the micro-grinding forces and surface roughness. The simulated forces and surface roughness were compared with the experimental results. Both the simulated forces and surface roughness followed the same trends as the empirical results.
- Increasing the cutting speed decreased the grinding forces in both simulation and experimental results. A similar influence was seen for varying depth of cut. The higher depth of cut increased the grinding forces and surface roughness values in both simulation and experimental results. However; both empirical and simulation results showed that the feed rate does not influence the surface roughness significantly.
- The model predicted the mean tangential and normal grinding forces with a total error of 13.5 %. In the case of prediction of the ground surface roughness, although, the simulation results were matched with the experimental results in greater degree in the low cutting speed of 6 m/s, rather in the higher cutting speed (14 m/s) because the tool vibration which occurs at the higher cutting speeds was not considered in the model. The surface roughness was predicted at the cutting speed of 6 m/sec with the total error of 16% among the mean values.

- The model shows that the effects of process parameters and wheel surface conditions could be acceptably mapped to the process outputs, of course with a degree of accuracy and simplification. The modeling process can be applied, if the tool conditions (initially or after being worn) could be described as a function of the grain size, concentration, height and distribution. Further robustness tests of the model for different conditions and material are currently being performed.

6.3. Paper III

- The dressing overlap ratio and speed ratio are influential factors in the term of surface quality.
- Increasing the dressing overlap ratio improved the surface roughness in both micro and macro-grinding processes and led to lower chip loading on the surface of the grinding pin in micro-grinding process.
- Changing the dressing mode from down to up dressing could improve the surface roughness as well as reducing the welded clogging on the surface of the grinding pin in the micro-grinding process. A more even surface and almost no cold-welded clogging could be observed when up-dressing the grinding pins.
- Using lower quantities of the grinding speed ratios along with higher overlap ratio improved the surface roughness more compared to the combination of higher grinding speed ratio and higher overlap ratio in macro-grinding process, however, the effect of grinding speed ratio is neglectable.
- Decreasing the grinding feed rate decreased the value of the surface roughness.
- The superior fine surface roughness of Ra = 0.035 obtained by using relatively high dressing overlap ratio U_d = 60 in macro-grinding process.

7. Future Work

As mentioned in the introduction, modeling of the micro-grinding process is in its early stage. And the micro-grinding process is still not a well-understood process, especially in terms of surface integrity. The future work consists of two analytical and experimental investigations.

7.1. Modeling

Prediction of grinding forces and surface roughness based on the dressing parameters and tool topography has not been in the focus of analytical modeling. According to the experiments carried out during the licentiate, both the surface roughness and grinding forces are highly influenced by the dressing parameters. Varying the dressing overlap ratio and speed ratio changes the topography of the tool. Hence, dressing parameters must be considered as important factors in modeling of the grinding process. In the future, an experimental model, based on the dressing parameters and the active grains will be extracted and included in the analytical modeling. To this end, the micro-tool will be dressed using the dressing parameters mentioned in the study. After the dressing, a confocal picture from the whole grinding pin will be taken. Using the pictures, it will be possible to quantify the number of active grains that come into the contact with the workpiece during the grinding. Changing the dressing parameters influences the number of active grains. It enables to extract an equation based on the dressing parameters (including the dressing speed ratio and overlap ratio) and the number of active grains. This can be used and included in the analytical model to calculate the grinding forces.

7.2. Material characterization

The surface integrity plays a key role in part performance and its fatigue life. Therefore, the micro-grinding and dressing parameters must be carefully chosen and controlled to achieve a desired surface integrity. So far, the effect of these parameters on the surface integrity are still not fully investigated. In the next stage, the surface integrity of the parts will be examined under different conditions. The investigation of materials characterization – including, residual stresses, phase transformation, micro-hardness, grain size and phase fractions, in micro-grinding Ti6Al4V titanium alloys will be carried out. The chip thickness in micro-machining is in the same order of magnitude as the material grain size. Therefore, changing the micro-grinding process parameters as well as dressing parameters give rise to the anisotropic behavior of the multiphase materials and their deformation characteristics. Thus, their influences are the subjects of future study. For this purpose, two kinds of Ti6Al4V materials, Additive Manufactured (AM) titanium and conventional titanium, will be chosen. The phase transformation mechanism of the materials will be studied to find the fundamentals of the methodological and mechanical phenomena during micro-grinding operation. The information regarding the grain structure (size, shape, and distribution), grain boundary characteristics, crystal graphic texture, and phase distribution will be obtained.

8. Acknowledgment

The author would like to thank Professor Bahman Azarhoushang, director of the Institute of Precision Machining (KSF), Professor Peter Krajnik, director of the Centre for Metal Cutting Research (MCR) at Chalmers Univerity, and Professor Uta Klement, Head of Division Materials and Manufacture, Department of Industrial and Materials Science at Chalmers Univerity for their kind spervision, advices and supports, they have provided throughout the licentiate. The author would also like to thank all KSF members specially Mr. Daneshi and Mr. Zahedi for their kind guidance during this period. In particular the author would like to thank the Meister Abrasive company for providing the micro-grinding tools.

9. References

[1] Cheng K, Huo D. Micro-cutting: Fundamentals and applications / editors: Kai Cheng, Brunel University, UK, Dehong Huo, Newcastle University, UK.

[2] Aurich JC, Carrella M, Walk M. Micro grinding with ultra small micro pencil grinding tools using an integrated machine tool. CIRP Annals - Manufacturing Technology 2015;64(1):325–8.

[3] Park JB, Lakes RS. Biomaterials: An introduction / Joon Park, R.S. Lakes. 3rd ed. New York, N.Y.: Springer; 2007.

[4] Ferri Y, Piotrowski O, Chauvy P, Madore C, Landolt D. Two-level electrochemical micromachining of titanium for device fabrication. J. Micromech. Microeng. 2001;11(5):522–7.

[5] C Madore, D Landolt. Electrochemical micromachining of controlled topographies on titanium for biological applications. Journal of Micromechanics and Microengineering 1997;7(4):270.

[6] Parker ER, Rao MP, Turner KL, MacDonald NC. Bulk Titanium Microneedles with Embedded Microfluidic Networks for Transdermal Drug Delivery. In: 19th IEEE International Conference on Micro Electro Mechanical Systems, p. 498–501.

[7] Thepsonthi T, Özel T. Experimental and finite element simulation based investigations on micro-milling Ti-6Al-4V titanium alloy: Effects of cBN coating on tool wear. Journal of Materials Processing Technology 2013;213(4):532–42.

[8] Özel T, Thepsonthi T, Ulutan D, Kaftanoğlu B. Experiments and finite element simulations on micro-milling of Ti–6Al–4V alloy with uncoated and cBN coated micro-tools. CIRP Annals 2011;60(1):85–8.

[9] Elias CN, Lima JHC, Valiev R, Meyers MA. Biomedical applications of titanium and its alloys. JOM 2008;60(3):46–9.

[10] Brunette DM, Tengvall P, Textor M, Thomsen P (eds.). Titanium in medicine: Material science, surface science, engineering. [Place of publication not identified]: Springer; 2013.

[11] Aimi MF, Rao MP, MacDonald NC, Zuruzi AS, Bothman DP. High-aspect-ratio bulk micromachining of titanium. Nature materials 2004;3(2):103.

[12] O'Mahony C, Hill M, Hughes PJ, Lane WA. Titanium as a micromechanical material. Journal of Micromechanics and Microengineering 2002;12(4):438.

[13] Parker ER, Thibeault BJ, Aimi MF, Rao MP, MacDonald NC. Inductively Coupled Plasma Etching of Bulk Titanium for MEMS Applications. J. Electrochem. Soc. 2005;152(10):C675.

[14] Parker ER, Thibeault BJ, Aimi MF, Rao MP, MacDonald NC. Inductively coupled plasma etching of bulk titanium for MEMS applications. Journal of the Electrochemical Society 2005;152(10):C675-C683.

[15] Anstis GR, Chantikul P, Lawn BR, Marshall DB. A critical evaluation of indentation techniques for measuring fracture toughness: I, direct crack measurements. Journal of the American Ceramic Society 1981;64(9):533–8.

[16] Donachie MJ. Titanium: A technical guide. 2nd ed. Materials Park, OH: ASM International; 2000.

[17] Jahan MP, Kakavand P, Kwang ELM, Rahman M, Wong YS. An experimental investigation into the micro-electro-discharge machining behaviour of aluminium alloy (AA 2024). Int J Adv Manuf Technol 2015;78(5-8):1127–39.
[18] Pradhan BB, Masanta M, Sarkar BR, Bhattacharyya B. Investigation of electro-discharge micro-machining of titanium super alloy. Int J Adv Manuf Technol 2009;41(11-12):1094–106.
[19] Pradhan BB, Masanta M, Sarkar BR, Bhattacharyya B. Investigation of electro-discharge micro-machining of titanium super alloy. The International Journal of Advanced Manufacturing Technology 2009;41(11-12):1094.
[20] Schomburg WK, Scherrer B. 3.5 mu m thin valves in titanium membranes. Journal of Micromechanics and Microengineering 1992;2(3):184.
[21] Yang L. The micro-air-vehicle Golden Snitch and its figure-of-8 flapping. 淡江理工學刊 2012;15(3):197–212.
[22] Ehmann KF, Bourell D, Culpepper ML, Hodgson TJ, Kurfess TR, Madou M et al. Micromanufacturing: International research and development. Springer Science & Business Media; 2007.
[23] Chae J, Park SS, Freiheit T. Investigation of micro-cutting operations. International Journal of Machine Tools and Manufacture 2006;46(3-4):313–32.
[24] Gäbler J, Pleger S. Precision and micro CVD diamond-coated grinding tools. International Journal of Machine Tools and Manufacture 2010;50(4):420–4.
[25] Cao XD, Kim BH, Chu CN. Hybrid micromachining of glass using ECDM and micro grinding. Int. J. Precis. Eng. Manuf. 2013;14(1):5–10.
[26] Zhou Y, Gong Y, Cai M, Zhu Z, Gao Q, Wen X. Study on surface quality and subsurface recrystallization of nickel-based single-crystal superalloy in micro-grinding. Int J Adv Manuf Technol 2017;90(5-8):1749–68.
[27] Feng J, Kim BS, Shih A, Ni J. Tool wear monitoring for micro-end grinding of ceramic materials. Journal of Materials Processing Technology 2009;209(11):5110–6.
[28] Feng J, Chen P, Ni J. Prediction of surface generation in microgrinding of ceramic materials by coupled trajectory and finite element analysis. Finite Elements in Analysis and Design 2012;57:67–80.
[29] Butler-Smith PW, Axinte DA, Daine M. Solid diamond micro-grinding tools: From innovative design and fabrication to preliminary performance evaluation in Ti–6Al–4V. International Journal of Machine Tools and Manufacture 2012;59:55–64.
[30] Lee P, Nam JS, Li C, Lee SW. An experimental study on micro-grinding process with nanofluid minimum quantity lubrication (MQL). Int. J. Precis. Eng. Manuf. 2012;13(3):331–8.
[31] Krajnik P, Rashid A, Pušavec F, Remškar M, Yui A, Nikkam N et al. Transitioning to sustainable production – part III: Developments and possibilities for integration of nanotechnology into material processing technologies. Journal of Cleaner Production 2016;112:1156–64.
[32] Perveen A, San WY, Rahman M. Fabrication of different geometry cutting tools and their effect on the vertical micro-grinding of BK7 glass. Int J Adv Manuf Technol 2012;61(1-4):101–15.

[33] Morgan C, Vallance RR, Marsh ER. Micro Grinding Blind Holes in Hard Tungsten Carbide with Polycrystalline Diamond Micro Tools.
[34] Morgan CJ, Vallance RR, Marsh ER. Micro machining glass with polycrystalline diamond tools shaped by micro electro discharge machining. J. Micromech. Microeng. 2004;14(12):1687–92.
[35] Morgan CJ, Vallance RR, Marsh ER. Specific grinding energy while microgrinding tungsten carbide with polycrystalline diamond micro tools. In: ICOMM-2007 2nd International Conference on Micro-Manufacturing; 2007, p. 180–187.
[36] Gong YD, Wen XL, Yin GQ, Wang C, Cheng J, Li BP. Experiment Research on Grinding Temperature of Micro-Grinding H62. AMR 2013;797:615–21.
[37] Ehmann KF, Kapoor SG, DeVor RE, Lazoglu I. Machining Process Modeling: A Review. J. Manuf. Sci. Eng. 1997;119(4B):655.
[38] Brinksmeier E, Aurich JC, Govekar E, Heinzel C, Hoffmeister H, Klocke F et al. Advances in Modeling and Simulation of Grinding Processes. CIRP Annals 2006;55(2):667–96.
[39] Tönshoff HK, Peters J, Inasaki I, Paul T. Modelling and Simulation of Grinding Processes. CIRP Annals 1992;41(2):677–88.
[40] Bissacco G, Hansen HN, Slunsky J. Modelling the cutting edge radius size effect for force prediction in micro milling. CIRP Annals 2008;57(1):113–6.
[41] Vogler MP, DeVor RE, Kapoor SG. On the Modeling and Analysis of Machining Performance in Micro-Endmilling, Part I: Surface Generation. J. Manuf. Sci. Eng. 2004;126(4):685.
[42] Park HW, Liang SY. Force modeling of micro-grinding incorporating crystallographic effects. International Journal of Machine Tools and Manufacture 2008;48(15):1658–67.
[43] Bhateja C. Grinding, theory, techniques, and troubleshooting. Society of Manufacturing Engineers; 1982.
[44] Anandita S, Mote RG, Singh R. Stochastic analysis of microgrinding tool topography and its role in surface generation. Journal of Manufacturing Science and Engineering 2017;139(12):121013.
[45] Kunz JA, Mayor JR. Stochastic Characteristics in Microgrinding Wheel Static Topography. Journal of Micro and Nano-Manufacturing 2014;2(2):21001.
[46] Gorodkova AE, Dyakonov AA, Herreinstein AV. Thermophysical modeling of microgrinding. Russ. Engin. Res. 2017;37(7):647–50.
[47] Feng BF, Cai GQ. Experimental Study on the Single-Grit Grinding Titanium Alloy TC4 and Superalloy GH4169. KEM 2001;202-203:115–20.
[48] Malkin S, Guo C. Grinding technology: theory and application of machining with abrasives. Industrial Press Inc; 2008.
[49] Zahedi A. Improving the Cylindrical Grinding of Engineering Ceramics by Applying Ultrasonic Vibrations and Laser Dressing,. Dissertation, Sharif University of Technology, Tehran, Iran. 2015.
[50] Yang CY, Xu JH, Ding WF. Grinding Force in Creep Feed Grinding of Titanium Alloy with Monolayer Brazed CBN Wheels. AMR 2012;565:94–9.
[51] Zahedi A, Azarhoushang B. FEM Based Modeling of Cylindrical Grinding Process Incorporating Wheel Topography Measurement. Procedia CIRP 2016;46:201–4.
[52] Shaw MC. Principles of abrasive processing. Oxford: Clarendon; 1996.

[53] Transchel R, Stirnimann J, Blattner M, Bill B, Thiel R, Kuster F et al. Effective Dynamometer for Measuring High Dynamic Process Force Signals in Micro Machining Operations. Procedia CIRP 2012;1:558–62.
[54] Azarhoushang B. Das Abrichten als integraler Bestandteil des Schleifprozesses: Unkonventionelle Abrichtprozesse. diamond business 2014;Heft 50(ISSN 1619 - 5558):82–9.
[55] Srivastava UM. Review of dressing and truing operations for grinding wheels. International Journal of Engineering Science and Technology;1(5):8–19.
[56] Rasifard A. Ultraschallunterstütztes Abrichten von keramisch gebundenen CBN-Schleifscheiben mit Formrollen. Shaker; 2011.
[57] Daneshi A, Jandaghi N, Tawakoli T. Effect of Dressing on Internal Cylindrical Grinding. Procedia CIRP 2014;14:37–41.
[58] Malkin S, Murray T. Mechanics of Rotary Dressing of Grinding Wheels. J. Eng. for Industry 1978;100(1):95.
[59] Murray T, Malkin S. Effects of Rotary Dressing on Grinding Wheel Performance. J. Eng. for Industry 1978;100(3):297.
[60] Linke B. Dressing process model for vitrified bonded grinding wheels. CIRP Annals - Manufacturing Technology 2008;57(1):345–8.
[61] Klocke F, Linke B. Mechanisms in the generation of grinding wheel topography by dressing. Prod. Eng. Res. Devel. 2008;2(2):157–63.
[62] Linke B, Klocke F. Temperatures and wear mechanisms in dressing of vitrified bonded grinding wheels. International Journal of Machine Tools and Manufacture 2010;50(6):552–8.
[63] Saad A, Bauer R, Warkentin A. Investigation of single-point dressing overlap ratio and diamond-roll dressing interference angle on surface roughness in grinding. Transactions of the Canadian Society for Mechanical Engineering 2010;34(2):295–308.
[64] Dražumerič R, Badger J, Klement U, Krajnik P. Truing of diamond wheels – Geometry, kinematics and removal mechanisms. CIRP Annals 2018;67(1):345–8.
[65] Tawakoli T, Rasifard A. Dressing of grinding wheels. In: Machining with Abrasives. Springer; 2011, p. 181–244.
[66] Wegener K, Hoffmeister H, Karpuschewski B, Kuster F, Hahmann W, Rabiey M. Conditioning and monitoring of grinding wheels. CIRP Annals - Manufacturing Technology 2011;60(2):757–77.
[67] Azarhoushang B. Intermittent Grinding of Ceramic Matrix Composites: Unterbrochenes Schleifen Von Keramischen Faserverbundwerkstoffen. Shaker; 2011.
[68] Malkin S. Grinding technology: Theory and applications of machining with abrasives. Dearborn, Michigan: Society of Manufacturing Engineers; 1989.
[69] Azarhoushang B, Tawakoli T. Development of a novel ultrasonic unit for grinding of ceramic matrix composites. Int J Adv Manuf Technol 2011;57(9-12):945–55.
[70] Malkin S. Grinding technology: Theory and applications of machining with abrasives. Dearborn, Michigan: Society of Manufacturing Engineers; 1989.
[71] Zhou Y, Gong Y, Cai M, Zhu Z, Gao Q, Wen X. Study on surface quality and subsurface recrystallization of nickel-based single-crystal superalloy in micro-grinding. Int J Adv Manuf Technol 2016;55(2):745.

[72] Wimmer J. Konditionieren hochharter Schleifscheiben zum Schleifen von Hochleistungskeramik. Lehrst. für Fertigungstechnik und Betriebsorganisation der Univ; 1995.
[73] Tawakoli, T., Daneshi, A (ed.). Innovative Abrichtrolle mit Punktkontakt optimiert die Abrichtprozesse, T-Dress,: Neue Entwicklungen und Trends aus Forschung und Praxis ; 9. Seminar "Moderne Schleiftechnologie und Feinstbearbeitung" am 15.05.2012 in Stuttgart. Villingen-Schwenningen: Hochsch. Furtwangen Abt. Villingen-Schwenningen; 2012.
[74] Wang W, Kweon SH, Yang SH. A study on roughness of the micro-end-milled surface produced by a miniatured machine tool. Journal of Materials Processing Technology 2005;162-163:702–8.
[75] Li B, Ding Z, Xiao J, Liang SY. Maraging steel 3J33 phase transformation during micro-grinding. Materials Letters 2016;164:217–20.
[76] Shamray S, Daneshi A, Azarhoushang B. High Efficiency, High Speed Grinding of a Composite Material Consisting of Polymer Concrete and Steel Structures. Procedia CIRP 2016;46:607–10.
[77] Arif M, Rahman M, Yoke San W. Analytical model to determine the critical feed per edge for ductile–brittle transition in milling process of brittle materials. International Journal of Machine Tools and Manufacture 2011;51(3):170–81.
[78] Kadivar MA, Akbari J, Yousefi R, Rahi A, Nick M. Investigating the effects of vibration method on ultrasonic-assisted drilling of Al/SiCp metal matrix composites. Robotics and Computer-Integrated Manufacturing 2014;30(3):344–50.
[79] Fujimoto M, Ichida Y. Micro fracture behavior of cutting edges in grinding using single crystal cBN grains. Diamond and Related Materials 2008;17(7-10):1759–63.
[80] Heinzel C, Antsupov G. Prevention of wheel clogging in creep feed grinding by efficient tool cleaning. CIRP Annals - Manufacturing Technology 2012;61(1):323–6.